Coupled Ocean-Atmosphere Variability in the Tropical Atlantic Ocean

Bohua Huang, Paul S. Schopf, and J. Shukla

January 28, 2003

Center for Ocean-Land-Atmosphere Studies
Institute of Global Environment and Society
4041 Powder Mill Road, #302
Calverton, Maryland 20705

Abstract

A rotated empirical orthogonal function analysis of the observed seasonal mean sea surface temperature (SST) anomalies for 1950-1998 shows that the tropical Atlantic variability is composed of three major patterns. They are the Southern Tropical Atlantic (STA) Pattern with SST fluctuations expanding from the Angola coast to the central equatorial ocean; the Northern Tropical Atlantic (NTA) Pattern centered near the northern African coast; and the Southern Subtropical Atlantic (SSA) Pattern in the open subtropical ocean. Each of these patterns has significant climate effects. Previous studies have suggested that both the regional air-sea coupling and remote forcing from outside the basin may affect the formation of these patterns and their variability.

A specially designed global coupled ocean-atmosphere general circulation model, which eliminates air-sea feedback outside the Atlantic, reproduced the patterns of these observed modes realistically. This suggests that these patterns can be produced by air-sea coupling within the Atlantic Ocean or by the oceanic responses to atmospheric internal forcing, in which there is no external anomalous SST forcing. The effect of the Pacific El Niño/Southern Oscillation (ENSO) seems to modulate their temporal evolution through influencing atmospheric planetary waves propagating into the basin.

Further analyses show that a typical NTA or SSA episode starts from the weakening of trade winds over the subtropical ocean, with associated anomalous surface heat fluxes forcing initial SST anomalies there. These initial SST anomalies then trigger an air-sea feedback among the wind speed, heat flux, and SST, which enhances the anomalies and move them into the tropical and equatorial ocean. The anomalies persist in the tropics during the next one to two seasons and are damped out when the heat flux anomalies change sign. The initial trade wind fluctuation in the subtropics is a part of the anomalous fluctuations of the subtropical anticyclones, which are connected with extra-tropical atmospheric disturbances. For NTA, the disturbances are mostly associated with low-frequency Rossby waves propagating from the eastern North Pacific and the North American continent. The SSA, on the other hand, is connected to the fluctuations in the mid-latitude westerlies that likely originate from the Antarctic Oscillation.

The coupled model also suggests that the STA pattern is driven by the dynamical response of the oceanic thermocline to the surface wind forcing. However, the model STA is much weaker than the observed because its equatorial fluctuations and the thermocline changes near the northeastern part of the ocean are largely unconnected. This lack of connection between these two parts of the tropical ocean is related to a model systematic bias, which shifts the inter-tropical convergence zone into the southern Atlantic in boreal spring. As a result, the warm water formed to the south of the equator weakens the local trade winds and easterlies on the equator. It also blocks the equatorial fluctuations from penetrating into the southern ocean effectively. Due to this systematic bias, this model did not simulate the tropical dynamical air-sea interactions adequately.

1. Introduction

There is substantial evidence linking the sea surface temperature anomalies (SSTA) of the tropical Atlantic Ocean to climate fluctuations in its surrounding regions. The best example may be northeast Brazil, where rainfall anomalies are statistically associated with an Atlantic SSTA "dipole" pattern straddling the climatological location of the Atlantic inter-tropical convergence zone (ITCZ, see e.g., Hastenrath and Heller 1977; Moura and Shukla 1981; and Nobre and Shukla 1996). Similar inter-hemisphere SSTA asymmetry has also been found in composites of major dry and wet years of sub-Saharan Africa (e.g., Lamb 1978a,b; Lough 1986; Lamb and Pepler 1991, and Folland et al., 1993).

More recent studies suggest that this dipole configuration reflects the fluctuation of the meridional SST gradient near the equator. Moreover, the gradient changes are usually triggered by the equator-ward extensions of the SSTAs originated from either north or south, which are largely unrelated with each other (Houghton and Tourre 1992; Enfield and Mayer 1997; Mehta 1998; Enfield et al., 1999). Therefore, the origination of SSTA in the northern and the southern tropical oceans, somewhat different from previously expected, may be due to different ocean-atmosphere processes and needs further investigation.

Figure 1 shows the patterns of the three leading modes of the rotated empirical orthogonal function (REOF) from the observed seasonal mean SSTA for 1950-1998 in the tropical Atlantic. The 1st mode (Fig.1a) is characterized by SST fluctuations centered near the Angola coast, which extend toward the central equatorial ocean and the Gulf of Guinea, usually referred to as the Southern Tropical Atlantic (STA) Pattern. The 2nd mode (Fig.1b) presents SST anomalies centered near the African coast in the northern tropical Atlantic Ocean; we refer to it as the Northern Tropical Atlantic (NTA) Pattern. The 3rd REOF mode (Fig.1c) shows SSTA fluctuations in the open ocean of the subtropical South Atlantic, to be referred to as the Southern Subtropical Atlantic (SSA) Pattern. Both the NTA and STA are well known patterns of the tropical Atlantic variability. However, not much attention has been paid to SSA yet even though it is a part of the

dominant SST fluctuation in the subtropical South Atlantic Ocean (Venegas et al., 1997). We refer to the variations associated with these three modes as the tropical Atlantic variability (TAV).

Apart from collectively forming an anomalous meridional gradient, there is also evidence that NTA, STA, and SSA all affect the regional climate individually. Year-to-year rainfall fluctuations in the Gulf of Guinea (Wagner and da Silva 1994) and Angola (Hirst and Hastenrath 1983) are associated with the STA fluctuations. The NTA, together with the El Niño/Southern Oscillation (ENSO) cycle in the Pacific, modulates rainfall in the Caribbean-Central America region (Hastenrath 1976, 1984; Enfield 1996; Enfield and Alfaro 1999; Giannini et al., 2000). Robertson and Mechoso (2000) found that the SSA-type SSTA fluctuations are correlated with the interannual variability of the South Atlantic Convergence Zone (SACZ). These relationships are the major sources of the climate predictability on seasonal to interannual time scales in the tropical Atlantic sector (Hastenrath et al., 1984; Hastenrath 1990; Ward and Foland 1991).

Current hypotheses on the mechanisms that generate the low frequency interannual ocean-atmosphere processes in the tropical Atlantic region can be classified into two complementary categories. One is regional ocean-atmosphere interaction and the other is the effect of the remotely generated atmospheric or oceanic low-frequency disturbances. It should be pointed out that both of these processes should have relatively high predictability from seasonal to interannual time scales. On the other hand, the atmospheric internal variability, which is less predictable on these time scales, may also affect these SSTA patterns significantly (Dommenget and Latif 2000).

For regional interaction, two air-sea feedback processes have been proposed. Chang et al. (1997) found a decadal oscillation in a hybrid-coupled model of the tropical Atlantic Ocean (an ocean model coupled with a statistical atmosphere). Its positive air-sea feedback involves surface wind speed, evaporation, and SST, usually referred to as the WES feedback (Xie 1999). Zebiak (1993) showed an interannual oscillation in the equatorial Atlantic using an intermediate ocean-

atmosphere model. Its structure suggests a positive feedback among the equatorial zonal wind, thermocline tilting and the SST, in a way similar to that of the Pacific ENSO (Zebiak and Cane, 1987). It will be referred to as the ZTS feedback in later discussions.

The WES and ZTS feedback mechanisms explain different aspects of the TAV. WES is a local interaction between the ocean mixed layer and the atmospheric low-level winds and is probably most suitable for explaining the tendency of the NTA anomalies to extend into the deep tropics in the western Atlantic (Chang et al. 2000; 2001). ZTS involves equatorial oceanic wave dynamics and provides a mechanism for the anomalous events in the Gulf of Guinea (Servain et al., 1982; Hirst and Hastenrath 1983, Carton and Huang 1994; Huang et al., 1995; Huang and Shukla 1997; Latif and Grötzner 2000). A common character of these two feedback mechanisms, however, is that the coupled oscillations in both models are not sustainable by themselves and need to be revitalized by external forcing factors.

Two major remote factors that influence TAV are ENSO and the North Atlantic Oscillation (NAO). There is extensive observational evidence of ENSO effects on TAV. For instance, observations showed that warm NTA usually appear a few months after the mature phase of the Pacific El Niño (Hastenrath et al., 1984; Curtis and Hastenrath 1995; Harzallah et al., 1996; Enfield and Mayer 1997; Roy and Reason 2001; Czaja et al., 2002). ENSO also tends to lead the SSTA in the Gulf of Guinea for a longer period (Horel et al. 1986; Delecluse et al., 1994; Carton and Huang 1994; Latif and Barnett 1995; Latif and Grötzner 2000; Jury et al., 2000). Moreover, it has been found that ENSO induced atmospheric wave trains, which originated from the western Pacific, may affect South Atlantic SSTA (Mo and Häkkinen 2001). On the other hand, possible extra-tropical effects, especially those on NTA from further north through NAO, have been documented by some observational and model studies, especially on longer time scales (e.g., Tourre et al., 1999; Tanimoto and Xie 1999; Häkkinen and Mo 2002; Czaja et al., 2002).

Therefore, it is unlikely that we can explain TAV through a single dominant mechanism like the one for ENSO in the tropical Pacific. Instead, we must examine the roles played by each of

the potential factors to understand its contributing mechanism to the observed SSTA patterns shown in Fig.1. The identification of their effects using observed data, however, is limited by the substantial overlap between the spatial patterns of the forced and coupled signals in the tropical Atlantic region (e.g., Saravanon and Chang 2000; Chang et al., 2001). This overlap makes it almost impossible to unambiguously find which process is at work and different studies seem to get contradictory results. Examining historical data, Czaja et al., (2002) suggested that most NTA peaks in the past few decades could be accounted for by the effects of either ENSO or NAO and questioned whether regional coupled dynamics played any role at all. The simplified coupled models (e.g., Chang et al., 1997; Xie 1999), on the other hand, suggested that regionally coupled modes determine the spatial structure and/or time scales of the fluctuations. These models, however, probably overestimated the regional coupling. For instance, the statistical SST-wind relationships, used in the hybrid models to determine the atmospheric feedback to the model SST, also include the remotely induced wind disturbances, which, in reality, should not be classified as coupled signals. Another potential problem of the simple models is that they might neglect some physical mechanisms that are relevant. Further studies based on more realistic models are needed to confirm their results.

In this paper, we analyze the TAV simulated by a coupled ocean-atmosphere general circulation model (CGCM), in which ocean-atmosphere coupling is included only within the Atlantic Ocean between 30°S-65°N. With this regional coupling strategy, one major potential remote-forcing factor to the tropical Atlantic, ENSO, is suppressed. Since there is no external SSTA forcing from outside the basin, the regional variability can only be generated by local air-sea coupling and/or oceanic responses to atmospheric internal variations. In this way, we can isolate the local signals from the strong remote ENSO effects and evaluate its development more accurately. Our results show that this regionally coupled model can reproduce the leading SST patterns shown in Fig.1, especially the NTA and SSA, quite realistically. This seems to suggest that these patterns can be produced by air-sea coupling within the Atlantic Ocean or by the

oceanic responses to atmospheric internal forcing, in which there is no external SST forcing. The main effect of ENSO may be primarily to modulate the temporal evolution of these modes through influencing atmospheric planetary waves propagating into the basin. Huang et al.(2002b) present a brief account of some preliminary results from this study.

The design of the simulation, including the CGCM and the regional coupling strategy, is described in the next section. The simulated mean state and annual cycle are presented in Section 3. The interannual variability is examined in Section 4. The ocean-atmosphere processes associated with these patterns are further analyzed in Section 5 through composite analyses. The summary and discussion are given in Section 6.

2. Experiment Design

The atmospheric and oceanic components of the CGCM are referred to as the AGCM and the OGCM respectively hereafter. The AGCM is Version 2 of the COLA AGCM as described in Schneider et al. (2001). It is a global spectral model, with a triangular truncation of the spherical harmonics at wave number 42, giving roughly a 2.8^o latitude x 2.8^o longitude resolution in the tropics. Vertically it is divided into 18 unevenly spaced σ levels with higher resolution in the lower troposphere. There is no sponge layer at the top levels. The model has the same dynamical core as that of the NCAR Community Climate Model version 3.0 (CCM3) and a semi-Lagrangian moisture transport scheme.

The AGCM's physical parameterizations include solar (Lacis and Hansen 1974; Davies 1982) and terrestrial (Harshvardhan et al., 1987) radiation schemes. The deep convection is parameterized by the Relaxed Arakawa-Schubert scheme (Moorthi and Suarez 1992), implemented in this model by DeWitt (1996). The shallow convection is by the scheme of Tiedke (1984) and the convective cloud fraction follows the scheme used in CCM3 (Kiehl et al., 1994). The Mellor and Yamada (1982) level 2.0 closure scheme is used for turbulent transport of heat, momentum, and moisture. There is also a parameterization of gravity wave drag (Palmer et al., 1986).

The OGCM is a nonlinear reduced gravity model of quasi-isopycnal layers, which is described in more detail in Schopf and Loughe (1995) and Yu and Schopf (1997). The model domain is the World Ocean within 70°S-65°N. It has 14 layers in the vertical and a horizontal resolution of 1°latitude x1.25°longitude while the meridional resolution is increased to 0.5° within 10°S-10°N to resolve the equatorial waves more accurately. The 1st model layer represents the well-mixed surface layer. The entrainment at its base is calculated through a balance of wind stirring, release of mean kinetic energy due to shear at the base of the layer, dissipation, and the increase in potential energy due to mixing, as set forth in Niiler and Kraus (1977). The internal shear-induced vertical mixing and diffusion are based on the Pacanowski and Philander's (1981) Richardson number-dependent scheme. There is also a convective overturning adjustment when the water column becomes statically unstable. Horizontal mixing is accomplished though a modified Shapiro (1970) filter, which is applied to the mass, temperature, and momentum fields.

Although both the OGCM and AGCM are global, they are fully coupled only in the Atlantic Ocean within 30°S-65°N for this study. Within the coupled region (Fig.2, red regions), the surface fluxes of heat, freshwater, and momentum at the sea surface simulated by the AGCM are provided to the OGCM at daily intervals. The OGCM simulated SST for the same interval is then supplied to the AGCM. Over the uncoupled portion of the global domain (Fig.2, purple regions), the SST is prescribed for the AGCM and the surface wind stress is prescribed for the OGCM. The net surface heat flux into the OGCM over the uncoupled portion of the global domain is given by the AGCM flux plus a relaxation term to the prescribed SST with a rate of $30 Wm^{-2} {}^{o}K^{-1}$. The fresh water flux is given from the AGCM output. A 10°-wide zone in the South Atlantic Ocean within 30°S-40°S is used to blend the coupled and uncoupled portions of the domain.

The prescribed data in the uncoupled domain for this simulation are the observed climatological monthly SST and wind stress fields. The former is derived from the U.S. Climate Prediction Center's (CPC) SST data for 1950-1998 (Smith et al., 1996) and the latter from the

National Centers for Environmental Prediction (NCEP) reanalysis (Kalnay et al., 1996). The ocean and atmosphere initial conditions used to initiate the coupled model are separately derived from long-term uncoupled simulations of these two component models. From this initial ocean-atmosphere state, the coupled run has been carried out for 200 years. The output from the last 110 years is used in this analysis.

3. Mean State and Annual Cycle

Before examining the interannual variability in the tropical Atlantic from the simulation, we first compare its mean state and annual cycle with observations. The mean states and annual cycles produced by coupled models for the tropical Pacific have been critically examined by many studies (e.g., Neelin et al., 1992; Mechoso et al., 1995; Schneider et al., 1997; Meehl et al., 1998). However, as far as we know, there have been no comparable examinations for the coupled tropical Atlantic simulations. We believe such an examination is relevant here because, as we will show later on, some potential problems in the model simulated interannual variability are closely related to the systematic errors in the mean field. Moreover, since the annual cycle is the dominant signal in the tropical Atlantic, a prerequisite of a successful model simulation of the regional climate variations should be that it reproduces the observed annual component.

The model reproduces the major features of observational SST and surface wind stress (Fig.3a,b) and net heat flux into the ocean (Fig.3c,d). On the other hand, the model and observations also have noticeable differences in some areas. For example, the observed net surface heat flux into the ocean is around 60-80 Wm^{-2} near the African coast around 10°N-20°N (Fig.3d), based on the estimate of the COADS climatology (da Silva, 1994), while the simulated flux is nearly zero there. The reason is the model has more cloudy skies in this region so that less solar radiative flux reaches the sea surface. The simulated regional mean SST, however, did not show a corresponding change (Fig.3e). The model SST, actually, is slightly warmer, possibly because the local upwelling, which is more sensitive to the local winds than the radiative heat flux, is the dominant factor there.

There is another model mean bias that has more serious consequences to its seasonal cycle and interannual variability. In the model, the warm water residing in the western ocean with mean temperature higher than 27°C penetrates toward the eastern boundary at around 5°S-15°S(Fig.3a). This penetration largely cuts off the link between the cold water in the eastern equatorial ocean and the coastal region further to the south, which collectively forms the observed cold tongue (Fig.3a, 3c). As a result, the simulation shows a positive SST error, larger than 3°C at its center near the eastern boundary at around 15°S, which extends northwestward to the equator (Fig.3e). This SST error reflects the climate drift of the coupled system, with the southeast trade winds weaker than the observed from the equator to around 15°S, located mostly to the south and west of the SST errors (Fig.3e). The simulated mean precipitation also features a strong center of precipitation (7mm day^{-1}) over the warm water belt around 5°S-10°S, which has no correspondence in observations.

This systematic error in the model's mean fields is closely connected to its annual cycle. The model and observations have a different latitudinal range of the seasonal migration of the ITCZ, as measured by the climatological monthly mean precipitation over the Atlantic Ocean (Fig.4). The observed ITCZ (panels in the left-hand column) shows an annual migration from near the equator in April (Fig.4c) to around 10°N in August (Fig.4g) and October (Fig.4i). The model ITCZ (panels in the right-hand column), on the other hand, is located at around 10°S from February (Fig.4b) to June (Fig.4f) when the model SST is warmest in this area. In June, a separate rainfall belt reappears in the model to the north of the equator over the Atlantic Ocean, which is then enhanced and moves northward to reproduce the observed location at 10°N from August (Fig.4h) to October (Fig.4j). During this period, the southern branch of the rainfall is weakened but persists near the coast of the South America (Fig.4h, j).

Scatterometer observations show July surface convergence at about the same location as the model's southern rainfall belt (Liu et al., 2002), which is attributed to shallow dry convections induced by weakening surface meridional winds from warmer water in the south to the equatorial

cold tongue. This is probably caused by changing vertical stability and mixing in the atmospheric boundary layer over warmer and colder waters. However, in the coupled model, this process usually triggers deeper convection, which in turn changes the SST and the ITCZ location. Moreover, the model produces strong southern precipitation in boreal spring and early summer, which is not observed in either the CPC analysis or the scatterometer data (Liu et al., 2002). This model rainfall pattern is similar to the migrating and sometimes double ITCZ feature of some coupled models in the tropical Pacific Ocean documented by Mechoso et al. (1995) and Meehl et al. (1998). As we have said above, it probably originates from inaccuracies in the parameterization of the convection in the tropics. Williamson et al. (1995) also demonstrated that, given the prescribed SST distribution, the simulation of the ITCZ is still sensitive to the resolution of the AGCM. Mechoso et al. (1995) pointed out that the effects of the stratus cloud, evaporation-wind feedback, and the coastal processes might all play some roles in this aspect. In a CGCM, the air-sea feedback amplifies these errors significantly and affects the mean ITCZ position.

Even though there is an ITCZ problem, the model still reproduces the annual strengthening of the easterlies in the western Atlantic starting from June and peaking at September (Fig.5a,b). This wind change corresponds to an enhancement and westward expansion of the cold water during the same period (Fig.5c,d). The warm up of the SST in the eastern ocean during boreal spring is also well reproduced. The simulated warming and cooling are about 1^{o}C larger than the observations. The excessive warming in boreal spring is due to the weaker easterlies over the central and eastern ocean because the strong southern ITCZ blocks the southeast trades from reaching the equatorial ocean (Fig.5a,b). Considering that both the model zonal and meridional wind stresses are weaker than the observations in boreal summer, the colder model SST suggests larger sensitivity to the changes of the surface stress, which is probably related to the model vertical mixing within the ocean. West of 40^{o}W, there is a secondary model easterly wind peak in February, which has no counterpart in the observations. This is caused by the northeast trades

penetrating to the equator associated with the southern bias of the ITCZ. This wind error, however, does not cause a significant SST change in the eastern ocean.

The model's annual harmonics of surface wind stress, heat flux, and the SST are largely consistent with observations in the tropical and subtropical region. In general, the amplitude of the model SST annual wave is larger than the observed while there is no such tendency in the winds and heat flux. This suggests that the model mixed layer is more sensitive to the surface forcing changes than the observed one. The model annual cycle is weak near the eastern part of the tropical ocean south of the equator at 5°S-15°S because the warm SST bias limits the expansion of the cold water from the eastern boundary.

Overall, the simulation produces qualitatively realistic mean fields of the SST, the surface wind stress, and the net surface heat flux in the fully coupled tropical Atlantic region. The model also simulates a realistic annual cycle with amplitude and phase largely comparable to the observations in most of the region. However, the model systematic error in the southern equatorial ocean has a significant effect on the patterns of the tropical Atlantic interannual variability, as we will see in the next section.

4. Major Interannual SSTA Modes

The observed standard deviation (STD) for SSTA, based on the 49-year CPC data, shows three major regions with standard deviation larger than 0.4°C (Fig.6a). These are the tropical North Atlantic and South Atlantic regions, both centered at the African coasts, as well as the subtropical South Atlantic in the open ocean. Significant variations (STD > 0.5°C) extend from the eastern boundary of the South Atlantic around 15°S to the central equatorial ocean, suggesting a strong connection between the variations in the southeast and those within the equatorial wave-guide. This STD distribution is consistent with the three leading REOF modes characterizing the NTA, the STA, and the SSA patterns (Fig.1). On the other hand, the lower SSTA STD (say, < 0.3°C) generally resides in the region with relatively higher mean SST (say, > 28°C, Fig.3a).

The coupled model qualitatively reproduced the three observed centers of variability (Fig.6a,b). The magnitude of the model STD is generally a little higher than the observed, as in the case of the annual cycle. A major discrepancy of the model from the observations is a zonal belt of low STD centered on 10°S, extending eastward. It is clearly associated with the higher model mean SST in this region. Its effect is the separation of the high STD region near the southeastern boundary into two parts, one around the equator and the other near 20°S. In particular, the model equatorial SSTA variability near the eastern coast is higher than the observed. Also like the annual cycle, the STD of model zonal wind stress anomalies is generally smaller than observed (not shown).

Our REOF analysis of the model SSTA shows that the leading SST patterns shown in Fig.1 can be reproduced quite realistically by this regionally coupled model (Fig.7). In particular, the 1st (Fig.7c) and 2nd REOF modes (Fig.7b) show spatial patterns that are very similar to the observed SSA (Fig.1c) and NTA patterns (Fig.1b). These two model modes explain a significant amount of the total variance (15.7% and 11.9% respectively) and their magnitudes are comparable to their observed counterparts (Fig.1b,c). This suggests that these patterns can be produced by air-sea coupling within the Atlantic Ocean or by the oceanic responses to atmospheric internal forcing, in which there is no external SST forcing. Moreover, these two patterns are very similar to the leading REOF modes of the annually averaged SSTA from several globally coupled GCM simulations shown in Demmonget and Latif (2000). The patterns of the two leading EOF modes of the simulated SSTA demonstrated by Cabosnarvaez et al. (2002) from the ECHAM4-OPYC3 coupled model (Roeckner et al., 1995) are also somewhat similar.

The 3rd model REOF mode, explaining about 9.3% of the total variances, depicts subtropical SSTA fluctuations centered on 30°N in the central part of the ocean, which is very similar to one of the higher REOF mode of the SSTA from the observations in spatial structure (not shown). However, we will not further discuss this mode because it is not significant in the observations. On the other hand, the spatial structure of the 4th model REOF mode (Fig.7a) is similar to the

observed STA pattern (Fig.1a), except that this model STA is more confined to the south of 10°S and explains much less of the total variance (7.7%) than the observed STA (25%). Hirst and Hastenrath (1983) suggested that the observed STA pattern is associated with air-sea interactions and oceanic waves in the equatorial wave-guide and is sensitive to the equatorial wind in the western and central Atlantic. The weak amplitude of its counterpart from the simulation suggests that the coupled model does not adequately simulate these equatorial processes. We suspect that this inadequacy is related to the warm mean SST bias to the south of the equator as described in last section and the fact that in the coupled model the ITCZ has two preferred locations. As in the annual cycle, this zone largely cuts off the link between the interannual fluctuations near the Angola coast and those within the equatorial wave-guide and splits them into two separate modes, as implied in the STD map (Fig.5b). In reality, however, they are closely connected (Fig.3a, see also, Hirst and Hastenrath 1983). A weak STA pattern seems to be a common feature of the CGCM simulations in the tropical Atlantic Ocean (e.g., Demmonget and Latif 2000). This issue will be further discussed in more detail later on when we further analyze the physical mechanisms of these modes.

The time series of the model STA, NTA, and SSA modes show similar statistical features with their observed counterparts. Power spectra of the STA and NTA from both the model (Fig.8a,b) and the observations (Fig.8e,f) follow very similar red noise distributions, consistent with what Demmenget and Latif (2000) have shown. All four of these time series show one season-lagged auto-correlation of 0.6. Both observed and model STA have local maxima at periods about 1.5 years that pass the 95% significance criteria (Fig.8a, d). For NTA, the observations show local peaks of variability at the periods of 2.5, 4, and 10 years. However, none of them are significantly distinguishable from the spectra of the red noise. The model shows local maxima at periods of 1.5 to 2 years that seem to be significant as well as a 4-year period and a much weaker peak at around 8 to 9-year periods.

Compared with the STA and NTA, both the model and observed SSA spectra are flatter (Fig.8c,f). Correspondingly, their auto-correlations at one-season's lag are also smaller, at 0.28 for the model and 0.47 for observations. For periods longer than one year, the observed spectrum has peaks with periods at around 5 and 16 years. The decadal period is similar to what Venegas et al. (1997) have found in their 1st SVD mode between SST and SLP in South Atlantic. The model, on the other hand, fluctuates mostly on interannual scales. There are three peaks that pass the 95% red noise significance level around 2.5, 1.5 and slightly less than 1 years in its spectrum. It is interesting to notice that there is a lack of lower frequency fluctuations in the model SSA in comparison with the observed one. A possible explanation is that there is no air-sea feedback south of 30°S and the lower frequency signals are suppressed.

We have further examined the REOF SSTA modes for each season separately. The observed NTA is dominant in boreal spring season (March-May), as pointed out by Nobre and Shukla (1996). Moreover, the center of the variations near the African coast migrates from 20°N-30°N in boreal summer and fall to 10°N-20°N in winter and spring. The percentage of the variances explained by the model NTA mode does not change as strongly with seasons as the observed. However, it does reproduce the observed meridional shift of the action center from season to season. On the other hand, the model SSA is dominant in austral summer (December-February), which is consistent with the observations. As for the STA, the observed mode is dominant in boreal summer (June-August), while the model mode is strongest in boreal fall (September-November). However, the equatorial SSTA fluctuations in the eastern Atlantic Ocean does appear as the 3rd mode in both the boreal summer and fall in the model. This SSTA variability is strictly trapped within 10°S-10°N and separated from the major center of STA, which is located at around 15°S near the African coast. This further demonstrates the effects of the model systematic bias on its patterns of the interannual variability.

5. Ocean-Atmosphere Processes

To further analyze the processes of the ocean-atmosphere interactions or the oceanic responses to the atmospheric forcing, which produce each of the three modes discussed in the last section, we conduct composite analyses of the relevant oceanic and atmospheric variables using indices based on the REOF modes.

1) NTA

For NTA composites, we chose the time series of the corresponding spring (MAM) season's REOF modes from both the observations (1st mode) and the simulation (2nd mode) as the base indices with the reason as discussed in last section. A positive or negative event was then defined as warm or cold SSTA pattern in the tropical North Atlantic Ocean as shown in Fig.7b. In particular, these events were selected from the peaks of these principal component time series, which have magnitudes larger than one standard deviation and are local maxima or minima within a two-year interval bracket. Before picking the events, we have removed a long-term trend from each of the time series so that the chosen events are relatively uniform in their distribution throughout the time series. This treatment makes the composite reflect the fluctuations on interannual time scales. 15 positive and 13 negative events were chosen from the simulation for the composites. In the 49-year data, only 5 positive and 5 negative events meet the criteria. The years of the positive events are 1958, 1966, 1969, 1983, and 1988. The years of the negative events are 1968, 1972, 1974, 1976, and 1985. In the following discussion, we examine the difference maps (positive minus negative composites) of the ocean-atmosphere variables between the positive and negative events in their corresponding months. We will emphasize the contrasting features between the positive and negative events, which pass a student-*t* test at a 95% confidence level.

Our examination of the differences identified some signals in the fall season (SON) proceeding the peak warming year, when an anomalous atmospheric cyclonic pattern forms in the central and eastern part of the North Atlantic, centered on 30^{o}N. Weakening trades cause an

anomalous heat flux of 10 to 15 Wm^{-2} into the ocean mainly in the eastern Atlantic between 10^oN-20^oN. At the same time, excessive heat loss occurs at 20^o-30^oN in the western to central Atlantic. These positive and negative heat flux anomalies induce weak positive and negative SSTA in their corresponding regions that are only marginally significant in the statistical test (not shown).

During the winter season (DJF), the wind signals initiated in fall are enhanced significantly, forming a pattern of weakened northeast trade wind in the tropics and cross equatorial atmospheric flow (Fig.9d). The anomalous surface heat fluxes are also strengthened, with the ocean gaining heat from the equator to 20^oN and losing heat from 30^oN to 40^oN (Fig.9g). At the surface, the tropics is warmed up, with a peak SST difference of 1.5^oC, and centered at around 10^oN near the African coast. The subtropics is cooled down, with a peak of 0.75^oC at 30^oN in open ocean (Fig.9a).

The area of warm SSTA ($>0.5^oC$) expands significantly from winter (DJF) to spring (MAM, Fig.9b), possibly due to the accumulating surface heat flux contributions since the winter season (Fig.9g). By the spring, although the anomalous cyclone in the extra-tropical atmosphere has largely disappeared, the basic features of the tropical winds persist, including the weakened trade winds in the subtropics and the cross equatorial flow further south (Fig.9e). However, the region of positive heat flux is weakened and confined in the central and western ocean, while near the African coast, the ocean starts to lose heat (Fig.9h). This longer persistence of the atmospheric and oceanic anomalies over the tropical ocean as well as the spatial structure of these variables suggests that the positive feedback as pointed out by Chang et al. (1997) and Xie et al. (1999) seems to be at work, especially in the west part of the ocean. The role played by this local feedback is not only to maintain or even enhance the anomalies but also to expand them toward the equator, as pointed out by Nobre and Shukla (1996) and Chang et al. (2001).

In the summer season (JJA), while the tropical SSTA pattern persists (Fig.9c), more changes occur to the surface fluxes. The most significant is the reversal of the anomalous wind directions

within the belt of 10°N-20°N from westerly in the spring (Fig.9e) to easterly in the summer (Fig.9f), even though the cross equatorial flow is maintained in the south. Moreover, the heat flux has become a damping term to the SSTA, which is negative in the tropics from the equator to 25°N where SSTA is positive, and positive around the Gulf Stream region where SSTA is negative (Fig.9i). With these damping effects, the SSTA pattern as seen in Fig.9c is expected to nearly disappear in the coming fall (SON) season.

We found that both the anomalous latent heat and the short-wave radiative fluxes play major roles in the evolution of the composite NTA event. The latent heat flux is the dominant force for heating up the northern tropical Atlantic and cooling down the extratropical ocean during winter (DJF). It is also responsible for the continued warming up of the western tropical and subtropical ocean in the following spring (MAM). Moreover, more solar radiation reaches the surface in the spring under the clear sky over the eastern Atlantic around 10°N, which causes net heat into the ocean there (Fig.9h). By the summer season, with the reversal of the trade wind anomalies in the subtropics, the anomalies of the latent heat flux change sign over the tropical region (Fig.10a). At the same time, anomalous solar radiation becomes a strong damping to the SSTA in the northern tropical Atlantic Ocean west of 40°W (Fig.10b). Some of the short-wave radiative effects are cancelled by the nearly opposite net long-wave radiative fluxes, which generally have magnitude less than half of the short-wave fluxes. The patterns of the anomalous radiative fluxes are connected to the increased convection and cloud cover over the warmer northern tropical Atlantic, especially in the central and western ocean (Fig.10d).

The model features as shown in Fig.9 are largely consistent with the composites of the chosen observational NTA events in the evolution of the SSTA and the surface wind stress (Fig.11). Especially in the decaying phase in the summer season, the observations show a strengthening of the easterly anomalies over the tropical-subtropical ocean (Fig.11f), as did the simulation (Fig.10f). This feature, together with the damping effects of the surface heat flux on SSTA in the "deep tropics", has not been emphasized in previous studies of model and observations. In

particular, this negative feedback through radiation has not been incorporated into any of the simple mechanistic models for the Atlantic variability. At the moment, it is hard to find observational evidence to evaluate how robust this feedback is as well as how important it is to the NTA process because long time series of high quality heat fluxes are not available. On the other hand, though relatively noisy, the heat flux maps from the NCEP/NCAR reanalysis show evolution of the large-scale features from the winter to the summer similar to those shown in Fig.9g-i.

The major difference between the simulation and observations is that the observed weakening of the northeast trade winds in the winter (DJF) during a warm NTA event is more confined to the subtropics north of 10^{o}N and is more intense over the western ocean (Fig.11d). The weakening of the trade winds in the central and eastern tropical Atlantic and the strong cross equatorial atmospheric flows occur mainly in the following spring (Fig.11e). Similarly, compared to the model patterns, the centers of the NCEP heat flux in the winter are shifted to the western subtropics. This pattern of atmospheric fluctuations seems to be consistent with the much larger increase of the observed SSTA in the tropical Atlantic from the boreal winter to spring (Fig.11a,b) and with the previous composite results by Nobre and Shukla (1996). Overall, it seems that the model NTA events peak earlier in the tropics than those from observations do. It is likely related to the model problem in the seasonal cycle because the large meridional shift of the ITCZ starts from the winter season, which should affect the wind there significantly. However, it should be emphasized that the simulated NTA events reproduced many features of the observed events and are largely consistent with the results from previous diagnostic studies by Hastenrath and Greischar (1993), Nobre and Shukla (1996), and Chiang et al.et al. (2002).

Previous studies have also emphasized the connection between the tropical Atlantic NTA fluctuations and the Pacific ENSO cycle (e.g., Enfield and Mayer 1997; Saravanan and Chiang 2000; Huang et al., 2002a; Czaja et al., 2002). However, the present experiment suggests that the spatial pattern of NTA is mainly determined by ocean-atmosphere coupling within the Atlantic

Ocean. The effect of ENSO may be primarily to modulate the temporal evolution of the NTA through influencing atmospheric planetary waves propagating into the basin. In fact, these NTA SSTA fluctuations in the model reflect the oceanic responses to the atmospheric disturbances associated with the subtropical high, which fluctuates significantly in the model even though there is no ENSO forcing.

Figure 12a shows the composite difference of the sea level pressure (SLP) anomalies during the boreal winter (DJF) when an NTA event is in its developing stage. The most significant feature in this composite is the anomalous trough centered at 35°N and 20°W-30°W, the climatological location of the subtropical high at this season. Associated with this weakened subtropical high is a cyclonic anomalous circulation with an equivalent barotropic vertical structure. Figure 12b and c show the zonal and meridional wind anomalies at 200hPa. Consistent with the patterns of the SLP (Fig.12a) and 200hPa geopotential height anomalies, the wind anomalies show westerlies to the south of 30°N and easterlies to its north, together with the southerly winds in the western Atlantic and northerly winds in the east. This tropospheric wind pattern is associated with the weakened trade winds near the surface (Fig.9d).

This structure of the atmospheric disturbances is reminiscent of the atmospheric low frequency fluctuations associated with Rossby wave propagation, as described by Hoskins and Karoly (1981). In particular, the wave train structure of the upper tropospheric meridional wind anomalies (Fig.12c) seems to trace the origins of these planetary waves to the west in the northeast Pacific and the North America continent (Jin and Hoskins 1995). Their centers of action, however, are somewhat different from the observed Pacific/North America (PNA) pattern (Wallace and Gutzler 1981). Although these model extratropical atmospheric patterns demonstrated here are qualitatively similar to what found by Nobre and Shukla (1996) based on their composite of the observed NTA events, the model SLP pressure and the 200hPa wind anomalies are apparently shifted eastward. Our own composite analysis of the observed NTA events as listed above, using the more recent NCEP/NCAR reanalysis data, shows a similar

difference with the model results. This shifting between the coupled model and the observations is possibly caused by the bias of the coupled model. On the other hand, it probably reflects the ENSO effects on the atmospheric planetary waves that propagate into the Atlantic basin in reality, which was absent in this particular model study.

We have also examined the relationship between the North Atlantic Oscillation (NAO) and the NTA variability. Although the NAO signals (defined as the 1st EOF mode of the SLP anomalies within the Atlantic sector in DJF) are quite strong in our model, its coefficients of the lagged correlation with the NTA index are generally low and statistically insignificant. It seems that in this model, the NAO effects on the NTA fluctuations are secondary and probably indirect, which is consistent with the recent modeling results of Wu et al. (2002).

2) SSA

The indices for the composites of the SSA events are the time series of the 1st and 3rd REOF modes of the austral summer (DJF) season for the simulated and observed SSTA. The spatial patterns of these two modes are very similar to those shown in Fig.1c and 7c and both are taken from the season when the SSA pattern explains the largest percentages of the total seasonal variances. The composite procedure is the same as we have described for the NTA case. For the observations, the samples for the composite warm event are the DJF season of 1598-59, 1966-67, 1968-69, 1970-71, 1972-73, 1982-83, and 1987-88. And those for the cold composites are: 1954-55, 1960-61, 1969-70, 1975-76, 1978-79, 1981-82, 1996-97.

Figure 13 shows the composite differences of the SSTA, surface wind stress and heat flux anomalies from the simulation during SON (1st column), DJF (2nd column), and MAM (3rd column). The situation is very similar to that of NTA. In austral spring (SON), there is broad weakening of the southeast trade winds over the tropical South Atlantic Ocean to the south of 10°S (Fig.13d), which causes anomalous surface heat flux of 10-20 Wm^{-2} into the ocean (Fig.13e). These surface forcing effects initiate positive SSTA in a broad belt between 20°S and 30°S (Fig.13a), which will be significantly enhanced to about 2.5°C in the next season (DJF,

Fig.13b). At the same time, cold SSTA appears to the south of 30°S, which forms an SSTA pattern similar to the north-south dipole with nodal line near 30°S described by Venegas et al. (1997). Furthermore, induced by the anomalous gradients associated with the SSTA, the northwest wind anomalies are strengthened further northward around 10°S-20°S (Fig.13e), which in turn enhance positive heat flux into the ocean there while the ocean starts to lose heat at 20°S-30°S (Fig.13h) due to the weakening local wind anomalies. The remaining westerly anomalies persist into the austral fall (MAM) in the central and eastern Atlantic around 10°S with the positive SSTA there (Fig.13c,f) while the southeast trade winds start to increase again further south in the western and central ocean, cooling down most of the southern ocean (Fig.13i). This process of the equator-ward expanding of both the SSTA and wind stress anomalies seems to be caused by an air-sea feedback where SSTA creates temperature and surface pressure gradients in the lower atmosphere that influence the low-level winds and wind stress. As a result, the changed winds affect and "move" the SSTA.

The initiation of an SSA warm event based on the observational data is very similar to what we have shown from the simulations (Fig.14a,b,d,e). However, it seems to end differently (Fig.14c,f). Instead of penetrating equatorward to the northeast, the SSTA dipole is maintained in the south while its center of the warm branch propagates westward to the South American coast (Fig.14b,c). By the austral fall, there are no major SSA signals existing in the wind field. These difference behaviors between the decaying phases of the model and the observed SSA composite events are not easy to explain. One should remember that the ocean model is only fully coupled with the atmospheric model south of 30°S and the meridional gradient of SSTA between 30°S-40°S is damped. This may affect the evolution of the model SSA events. The effect of this artificial boundary to the SSA simulation should be further investigated by comparing the results from this model with those from a globally coupled simulation.

The forcing of the SSA fluctuations seems also to originate from the extratropics, as was the case for the NTA events. Fig.15a presents the composite differences of the SLP anomalies in the

South Atlantic sector in austral summer (DJF) when the SSA anomalies are in their peak phase. The differences show an anomalous cyclonic circulation over the South Atlantic with the low-pressure center located at around 40°S-45°S and 10°W-20°W, which expands northwestward into the tropical region. Further to the south, the sea level pressure over Antarctic is anomalously high. In between these two centers, the meridional gradient between 50°S-70°S is very strong. It seems to be associated with the weakening of the westerlies in the mid-latitude as well as the subtropical high climatolgoically centered at 30°S at this season. The corresponding composite of the observational data (Fig.16a) shows a very similar pattern, except for a northward shift of the low-pressure center to about 50°S.

The vertical structure of the atmospheric disturbance is equivalent barotropic in the extratropical region, as shown by the geopotential height patterns at 850, 500, and 200hPa for both the simulation (Fig.15b,c,d) and observations (Fig.16b,c,d). In the subtropical region (south of 30°S) over the South Atlantic, however, the structure becomes baroclinic, with a ridge at the 200hPa appears over the trough at the 850hPa, as seen from both the model (Fig.15b,d) and observational (Foig.16b,d) composites. This suggests that the SSTA in the South Atlantic can affect the lower troposphere circulation regionally (Robertson et al., 2002). On the other hand, the basic structure of the extratropical atmospheric circulation is similar to the southern annualar modes as described by Fyfe et al.(1999), Gong and Wang (1999), Thompson and Wallace (2000) and Thompson et al (2000), which has been demonstrated by these previous studies as the leading mode of variability. Our results further suggest that these extratropical fluctuations may have strong influence in the tropical Atlantic region.

c) STA and the anomalous events in the Gulf of Guinea

The STA mode is a major signal existing year-around in the observed tropical Atlantic SST data. It is strongest, however, in the boreal summer when the equatorial fluctuations associated with the anomalous warm and cold events in the Gulf of Guinea are most active (e.g., Servain 1982; Hastenrath and Hirst 1983). Figure 17 shows the composite evolution of a typical STA

event from boreal spring to fall seasons, based on the time series of the 1st REOF mode of the boreal summer (JJA) SSTA from the observations with the same composite procedure as described before. The chosen years of warm events are 1951, 1963, 1966, 1974, 1984, and 1988. The cold-event years are 1954, 1958, 1967, 1976, 1983, and 1992.

In fact, the STA event is initiated in the DJF season when the weakening of the southeast trade winds over the southern tropical Atlantic causes increased SSTA in both the open ocean around 10°S-20°S and the African coast centered around 15°S (not shown). This trade wind weakening is associated with anomalous cyclonic atmospheric circulation in the southern subtropics, which is very similar to what happens at the peak phase of an SSA event. By the MAM season, the weakening southeast trades have penetrated into the equatorial ocean, causing anomalous northwesterlies over the equator and northerly winds to its north (Fig.17d). Associated with this wind pattern, there is nearly basin-wide warming in the southern tropical Atlantic (Fig.17a). The pattern of the SSTA, however, shows that there are two sources of its origination. One is located near the African coast near 20°S with a maximum around 2°C. It has been forced by the trade wind anomalies since DJF and linked with the warming between 10°S-20°S. Another center of variability is near the equator at around 15°W. This represents the oceanic response to the equatorial westerlies that causes the second branch of the westward expansion of the warming signals within the equatorial ocean.

It should be pointed out that, unlike the NTA and SSA events, both STA centers of activity have been generated through the dynamical responses of the ocean to the wind changes through thermocline adjustment while the heat flux effects are secondary. Fig.17g, h, and Fig.17i show the composite upper ocean heat content (mean temperature of the upper 234 meters) anomalies based on the observed anomalous events after 1958. The analyzed upper ocean temperature fields used for the composite come from an ocean data assimilation system as described in the appendix of Huang and Kinter (2002). They show that the largest SSTA off the African coast are associated

with the deepening of the thermocline and warming up of the upper ocean and the equatorial wind anomalies flatten the zonal tilting of the thermocline there (Fig.17g).

By the season of June-July-August (JJA), while the subtropical SSTA weakens, the equatorial SSTA has been further enhanced (Fig.17b). This is associated with the enhanced westerlies in the central and western equatorial Atlantic, which, together with the meridional atmospheric flow from both hemispheres, form a convergence zone around the equator (Fig.17e). The coastal warming signals are strengthened and move northward to near 10^{o}S. Hastenrath and Hirst (1983) have pointed out that westerly anomalies in the central and western equatorial Atlantic remotely force the thermocline fluctuations in the eastern boundary by generating eastward propagating Kelvin waves. The heat content anomalies (Fig.17h) shows that the further deepening of the thermocline in the Gulf of Guinea and the eastern boundary as well as the off-equatorial warm anomalies are probably the incoming Kelvin wave signals reflected from the eastern boundary and propagating slowly westward as Rossby signals. At the same time, there is also further shoaling of the thermocline in the western equatorial ocean off the South American coast. The warming in the east starts to decay in the boreal fall (SON, Fig.17c) when the equatorial wind is weakened and the convergence zone shifts to the south of the equator (Fig.17f). The off-equatorial oceanic signals also propagate away from the eastern ocean (Fig.17i).

The strengthening of the equatorial signals is associated with the ENSO-like air-sea feedback within the equatorial Atlantic Ocean, which has been examined in many previous studies (e.g., Zebiak 1993; Carton and Huang 1994; Huang et al., 1995; Huang and Shukla 1997; Latif and Grötzner 2000; CabosNarvaez et al., 2002). Based on an intermediate coupled model of the tropical ocean, Zebiak (1993) suggested that this equatorial Atlantic variability represents an intrinsic mode of the regional air-sea coupling with a period of 4 years, even though it is damped. On the other hand, Latif and Grözner (2000) showed the concentration of the energy around the biennial period in the observational data. They speculated that this two-year time scale is dictated by the delayed oscillator mechanism of the equatorial air-sea feedback process (Schopf and

Suarez 1988) in the given east-west width of the equatorial Atlantic Ocean. Latif and Barnnet (1995) and Latif and Grötzner (2002) also suggested that the outside forcing such as ENSO has a strong remote effect.

Figure 17, on the other hand, seems to suggest that the STA fluctuation, which is the leading mode of the tropical Atlantic SSTA, is not simply an equatorially confined phenomenon. The penetration of the basin-wide southeast trade wind anomalies into the equatorial ocean in the DJF to MAM seasons are important in initiating the equatorial oceanic response, which in turn enhances the off equatorial anomalies in the eastern ocean that have been generated before the equatorial warming started. It is this coupling between the equatorial and off-equatorial processes that generates this dominant signal in the southern tropical Atlantic Ocean. The pattern also suggests a potential connection with the SSA mode.

The coupled model, however, did not simulate this coupling between the equatorial and the southern tropical ocean adequately, which leads to a weak tropical southern Atlantic variability. The model STA mode is strongest in austral spring (SON), one season later than the observed peak. Our composite analysis based on the 2nd REOF mode of the model SON SSTA (Fig.18) shows that the model STA events is significantly weaker in its equatorial part than the observed, even though the evolution of the major variables are quite similar further to the south. In particular, the model southeast trade wind anomalies, already quite strong from austral summer (DJF) to fall (MAM), did not penetrate into the equatorial ocean until the boreal winter (JJA) season (Fig.18d,e). This delay prevents a coherent equatorial signal from occurring in JJA. This is related to the systematic bias of the model climatology in the MAM season, as we have discussed before.

On the other hand, the model produced a separate equatorial variability that is isolated from the STA mode. The composite based on the 3rd REOF mode of the JJA SSTA characterizes this equatorial fluctuation (Fig.19). Unlike the observed STA mode, the SSTA is mostly confined within the equatorial wave-guide and strong only in boreal summer (Fig.19a,b,c). The warming in

the summer was probably preconditioned by the thermocline deepening in the western equatorial ocean, both along and off the equator (Fig.19g). However, the large increase of the SSTA in the eastern equatorial ocean is forced by the equatorial westerlies over and to the north of the equator (Fig.19e), which cause the deepening of the thermocline in the eastern equatorial ocean (Fig.19h). In the boreal fall season, both the SSTA and the heat content anomalies are largest in the central equatorial ocean (Fig.19c,i). For the heat content field, the maxima are located a few degrees off the equator to both the north and south (Fig.19i), representing the westward propagating Rossby wave signals reflected from the eastern boundary. There are statistically significant wind stress anomalies in the subtropical South Atlantic before the warming is initiated (Fig.19d) and in the subtropical North Atlantic after the warming decays (Fig.19f). However, they seem not to affect the equatorial event directly.

We have further examined the temporal characteristics of the equatorial variability using the ATL3 index (SSTA averaged within 3°S-3°N, 0°-20°W) defined by Zebiak (1993). We find that both the model and observed SSTA fluctuations in the ATL3 region have similar seasonality, i.e., strongest in boreal summer. However, our power spectral analysis shows that observed ATL3 index has a "redder" spectrum than the model one does. The model events are more short-lived and have a higher frequency in occurrence. Whether this is caused by the lack of outside forcing within the model at the lower frequency band such as those from the ENSO cycle (e.g., Latif and Grötzner 2000) or by the split of the equatorial signals and the southern tropical variability needs to be further investigated.

6. Summary

The tropical Atlantic variability is composed of a variety of SST fluctuations in the subtropics, tropics, and the equatorial ocean. They are generated by different mechanisms of regional air-sea feedback, passive oceanic responses to atmospheric forcing, and remote connections to major climate variations in other parts of the world. Understanding the different roles played by these processes and their interactions in forming the SST variability we observed

is a major issue in understanding the nature of the climate variations in this region and its potential predictability. In this study, we used a specially designed global coupled ocean-atmosphere general circulation model to separate the effects of the regional air-sea coupling from remote forcing. In this model, the oceanic and atmospheric components are coupled with each other within the Atlantic Ocean between 30°S-65°N, while both are forced by prescribed mean annual cycle of the surface fluxes over the rest of the uncoupled oceanic basin. This arrangement removes a major potential remote source of the tropical Atlantic variability, the Pacific El Niño/Southern Oscillation (ENSO).

An examination of a 110-year simulation shows that the model reproduces the observed structure of the northern tropical Atlantic (NTA) and the southern subtropical Atlantic (SSA) modes. This implies that these patterns are determined by ocean-atmosphere coupling within the Atlantic sector and oceanic responses to internal atmospheric noise. Moreover, NTA or SSA evolution starts from the weakening of trade winds over the subtropical ocean, with associated anomalous surface heat fluxes forcing initial SSTA in the subtropical ocean. These initial SSTA then trigger an air-sea feedback among the wind speed, heat flux, and SST anomalies, which enhance the anomalies and move them into the tropical and equatorial ocean. The anomalies persist in the tropics during the next one to two seasons and are damped out when the heat flux anomalies change sign.

The initial trade wind fluctuation in the subtropics is a part of the set of anomalous fluctuations of the subtropical anticyclones, which are connected with extra-tropical atmospheric disturbances. For NTA, the disturbances are mostly associated with low-frequency Rossby waves propagating from the eastern North Pacific and the North American continent. The SSA, on the other hand, is connected to the fluctuations of the mid-latitude westerlies that probably originate from the Antarctic Oscillation.

The coupled model also reproduces some characteristics of the southern tropical Atlantic (STA) pattern composed of SST fluctuations from the Angolan coast to the Gulf of Guinea,

which represents a major mode in the observed data. This mode is mainly driven by the dynamical response of the oceanic thermocline to the surface wind forcing, instead of the heat flux fluctuations as in the NTA and SSA cases. However, the model STA is much weaker than the observed one because, unlike the observations, the equatorial fluctuations and the thermocline changes near the northeastern part of the ocean are largely unconnected. One question, then, is whether the lack of ENSO forcing and the possibly weaker effects from the southern extra-tropical ocean also played roles in the weak model STA. To answer the question of the ENSO effect, we have examined an experiment with observed SST is prescribed in the uncoupled region. We have also examined a globally coupled run where there are full interactions with the southern extra-tropical ocean. We did not see a significant change in the pattern and strength of the model STA in both cases. We thus conclude that the model systematic error is the main reason for a weak STA simulation. The lack of ENSO and extra-tropical effects is probably secondary.

This lack of connection between the equatorial and the southern tropical ocean is related to the model systematic bias, which produces weaker zonal winds near the equator and warmer SST to its south. This bias is linked to the seasonal shift of the inter-tropical convergence zone into the southern ocean in boreal spring. The warm water formed to the south of the equator seems to block the equatorial fluctuations from penetrating into the southern ocean effectively. Due to this systematic bias, this model did not simulate the tropical dynamical air-sea interactions adequately. It is also possible that model STA is weak partly due to the regional coupling, which eliminated the potentially important ENSO effects and the extra-tropical effects from the south. However, our other experiments with prescribed realistic ENSO signals in the Pacific as well as global full coupling didn't show an enhanced STA mode in the model. These suggest that these latter factors are at most secondary, in comparison with the effects of the model systematic bias.

These results on NTA and SSA modes are largely consistent with those derived by Dommenget and Latif (2000). Examining annual mean SST data from several globally coupled

ocean-atmosphere general circulation models (CGCM), they have pointed out that the surface heat flux fluctuations associated with the fluctuations of the subtropical anticyclones are a major mechanism causing the tropical Atlantic SST variability. In fact, the two leading REOF modes of our model simulation, the SSA (Fig.2c) and NTA (Fig.2b), are very similar to the two leading modes from the models Dommenget and Latif (2000) have shown (see their Fig.6).

However, our results differ from Dommenget and Latif's (2000) conclusion that major tropical Atlantic SST fluctuations passively respond to local atmospheric forcing. It seems to us that their analysis did not distinguish the fundamental difference between the STA and SSA fluctuations in the southern tropical and subtropical Atlantic Ocean. Consistent with our results, patterns similar to the observed SSA are found as a leading mode for all the coupled models reported in Dommenget and Latif's (2000). They further noticed that this mode from simulation is strongly affected by subtropical atmospheric fluctuations, fully consistent with of description of the SSA mode. However, Dommenget and Latif (2000) have interpreted this mode to be a counterpart of their observed leading mode in the southern ocean, which, in our opinion, is more similar to the STA then the SSA.

Therefore, it seems to be premature to conclude at this stage that the southern tropical Atlantic SST variability is mainly caused by heat flux forcing from the subtropics, while air-sea feedback and ocean dynamics have little effect. In fact, based on our analysis above, the contribution of the regional air-sea coupling and oceanic dynamics is significant for STA, which, in reality, accounts for much larger portion of the total variance than the SSA mode does. We also notice that, like our model, none of the model's analyzed by Dommenget and Latif (2000) showed an SSTA pattern in their first two leading REOF modes that is similar to the STA pattern as shown in Fig.1. A similar situation occurred in the coupled model analyzed by CabosNarvaez et al. (2002). It seems in many present coupled models the dynamic oceanic fluctuations represented by the STA mode are severely underestimated.

Our results demonstrate that the WES mechanism proposed by Chang et al. (1997, 2001) and Xie (2001) expand the subtropical SST anomalies into the western tropical Atlantic in the NTA evolution. It is probably the major mechanism that maintains the air-sea anomalies for a longer period in the tropical region after the initial anomalies disappeared in the subtropics. However, this process is strongly seasonal-dependent and only effective from late boreal winter to spring for NTA. Therefore, it may not be the major force to generate the decadal scale oscillation in the tropical Atlantic basin as demonstrated in Chang et al. (1997) using a more simplified model. One crucial mechanism of Chang et al.'s (1997) oscillatory mode is the slow negative feedback of the meridional currents, which allows the decadal time scale to be realized. However, our coupled model results seem to suggest that there are other negative feedback mechanisms, such as the cloud induced changes in solar radiative flux, which is more effective in damping out the SST anomalies in the tropics. For SSA, there is also a possibility that a similar WES feedback among the anomalies of SST, surface wind speed, and heat flux tends to move these anomalies from the subtropical ocean into the tropics, even triggering the STA-type anomalies by initiating equatorial wind fluctuations. This possibility needs to be further examined using both model and observational data sets.

In a previous study using the regional coupled model forced with observed SST in 1950-1998 over the uncoupled domain, Huang et al. (2002a) found significant ENSO influences on the NTA, which is similar to the observed ENSO-NTA relationship (Enfield and Mayer 1997). The present experiment suggests that the spatial pattern of NTA is mainly determined by ocean-atmosphere coupling within the Atlantic Ocean. The effect of ENSO may be primarily to modulate the temporal evolution of the NTA through influencing atmospheric planetary waves propagating into the basin.

Acknowledgments

This study is supported by grants (NA96GP0446 and NA169PI570) from National Oceanic and Atmospheric Administration's CLIVAR Atlantic Program. We would like to thank Dr. B.

Kirtman for helping us to develop the coupled model and Mr. Z. Pan for programming work. We would also like to thank Drs. Q. Wu and V. Krishnamurthy for discussions on the application of the spectral analysis and Drs. B. Klinger and D. Straus for editing the manuscript and making many useful comments for its revision.

References

CabosNarvaez, W., F.A. Garcia, and M.J. Ortizbevia, 2002: Generation of equatorial Atlantic warm and cold events in a coupled general circulation model simulation. *Tellus*, **54A**, 426-438.

Carton, J.A., and B. Huang, 1994: Warm events in the Tropical Atlantic. *J. Phys. Oceanogr.*, **24**, 888-903.

Chang, P., L. Ji, and R. Saravanan, 2001: A hybrid coupled model study of tropical Atlantic variability. *J. Climate*, **14**, 361-390.

Chang, P., R. Saravanan, L. Ji, and G.C. Hegerl, 2000: The effect of local sea surface temperatures on atmospheric circulation over the tropical Atlantic sector. *J. Climate*, **13**, 2195-2216.

Chang, P., L. Ji, and H. Li, 1997: A decadal climate variation in the tropical Atlantic Ocean from thermodynamic air-sea interactions. *Nature*, **385**, 516-518.

Curtis, S., and S. Hastenrath, 1995: Forcing of anomalous surface temperature evolution in the tropical Atlantic during Pacific warm events. *J. Geophys. Res.*, **100**, C8, 15,835-15,847.

Czaja, A., P. van der Vaart, and J. Marshall, 2002: A diagnostic study of the role of remote forcing in tropical Atlantic variability. *J. Climate*, **15**, 3280-3290.

da Silva, A.M., C. C.Young-Molling, and S. Levitus, 1994: Atlas of Surface Marine Data 1994, Vol. 1: Algorithms and Procedures. NOAA Atlas NESDIS 6. U.S. Gov. Printing Office, Wash., D.C*.,* 83 pp.

Davis, R., 1982: Documentation of the solar radiation parameterization in the GLAS climate model. NASA Technical Memorandum 83961, 57pp.

Delecluse, P., J. Servain, C. Levy, K. Arpe, and L. Bengtsson, 1994: On the connection between the 1984 Atlantic warm event and the 1982-1983 ENSO. *Tellus*, **46A**, 448-464.

DeWitt, 1996: The effect of the cumulus convection scheme on the climate of the COLA general circulation model. *COLA Tech. Report*, **27**, 58pp.

Dommenget, D., and M. Latif, 2000: Interannual and decadal variability in the tropical Atlantic. *J. Climate*, **13**, 777-792.

Enfield, D.B., 1996: Relationships of inter-American rainfall to tropical Atlantic and Pacific SST variability. *Geophys. Res. Lett.*, **23**, 3305-3308.

Enfield, D.B., and D. A. Mayer, 1997: Tropical Atlantic sea surface temperature variability and its relation to El Niño-Southern Oscillation. *J. Geophys. Res.*, **102**, 929-945.

Enfield, D.B., A.M. Mestas-Nuñez, D.A. Mayer, and L. Cid-Serrano, 1999: How ubiquitous is the dipole relationship in tropical Atlantic sea surface temperature? *J. Geophys. Res.*, **104**, 7841-7848.

Enfield, D.B., and E.J. Alfraro, 1999: The dependence of Caribbean rainfall on the interaction of the tropical Atlantic and Pacific Oceans. *J. Climate*, **12**, 2093-2103.

Folland, C., T. Palmer, and D. Parker, 1986: Sahel rainfall and worldwide sea surface temperatures. *Nature*, **320**, 602-606.

Fyfe, J.C., G.J. Boer, and G.M. Flato, 1999: The Arctic and Antarctic oscillations and their projected changes under global warming. *Geophys. Res. Lett.*, **26**, 1601-1604.

Giannini, A., Y. Kushnir, and M.A. Cane, 2000: Interannual variability of Caribbean rainfall, ENSO, and the Atlantic Ocean. *J. Climate*, **13**, 297-311.

Gong, D., and S. Wang, 1999: Definition of Antarctic oscillation index. *Geophys. Res. Lett.*, **26**, 459-462.

Häkkinen, S., and K.C., Mo, 2002: The low-frequency variability of the tropical Atlantic Ocean. *J. Climte*, **15**, 237-250.

Harzallah, A., J.O. Rocha De Aragao, and R. Sadourny, 1996: Interannual rainfall variability in northeast Brazil: observation and model simulation. *Int. J. Clim.*, **16**, 861-878.

Harshvardhan, R.. Davis, D.A. Randall, and T.G. Corsetti, 1987: A fast radiation parameterization for general circulation models. *J. Geophys. Res.*, **92**, 1009-1016.

Hastenrath, S., 1990: Prediction of northeast Brazil rainfall anomalies. *J. Climate*, **3**, 893-904.

Hastenrath, S., 1984: Interannual variability and annual cycle: Mechanisms of circulation and climate in the tropical Atlantic sector. *Mon. Wea. Rev.*, **112**, 1097-1107.

Hastenrath, S., 1976: Variations in low-latitude circulation and extreme climatic events in the tropical Americas. *J. Atmos. Sci.*, **23**, 604-711.

Hastenrath, S., and L. Heller, 1977: Dynamics of climate hazards in Northeast Brazil. *Quart. J. Roy. Meteor. Soc.*, **103**, 77-92.

Hirst, A., and S. Hastenrath, 1983: Atmosphere-ocean mechanisms of climate anomalies in Angola-tropical Atlantic sector. *J. Phys. Oceanogr.*, **13**, 1146-1157.

Horel, J.D., V.E. Kousky, and M.T. Kagaro, 1986: Atmospheric conditions in the tropical Atlantic during 1983 and 1984. *Nature*, **322**, 243-245.

Hoskins, B.J., and D.J. Karoly, 1981: The steady linear response of a spherical atmosphere to thermal and orographic forcing. *J. Atmos. Sci.*, **38**, 1178-1196.

Houghton, R.W., and Tourre, Y., 1992: Characteristics of low frequency sea surface temperature fluctuations in the tropical Atlantic. *J. Climate*, **5**, 765-771.

Huang, B., and J.L. Kinter III, 2002: The interannual variability in the tropical Indian Ocean. *J. Geophys. Res.*, **107**(C11), doi: 10:1029/2001JC001278, 3199.

Huang, B., P.S. Schopf, and Z. Pan, 2002a: The ENSO effect on the tropical Atlantic variability: A regionally coupled model study. *Geophys. Res. Lett.*, **29**(21), doi: 10:1029/2002GL014293, 2039.

Huang, B., P.S. Schopf, and J. Shukla, 2002b: Coupled ocean-atmosphere variability in the tropical Atlantic Ocean. *CLIVAR Exchanges*, **7**, No.3/4, 24-27.

Huang, B., and J. Shukla, 1997: Characteristics of the interannual and decadal variability in a general circulation model of the tropical Atlantic Ocean. *J. Phys. Oceanogr.*, **27**, 1693-1712.

Huang, B., J.A. Carton, and J.Shukla, 1995: A numerical simulation of the variability in the tropical Atlantic Ocean, 1980-88. *J. Phys. Oceanogr.*, **25**, 835-854.

Jin, F.F., and B.J. Koskins, 1995: The direct response to tropical heating in a baroclinic atmosphere. *J. Atmos. Sci*, **52**, 307-319.

Jury, M.R., H. Mulenga, and H. Rautenbach, 2000: Tropical Atlantic variability and Indo-Pacific ENSO: statistical analysis and numerical simulation. *Global Atmos. Ocean Sys.*, **7**, 107-124.

Kalnay, E., and coauthors, 1996: The NCEP-NCAR 40-year Reanalysis Project. *Bull. Amer. Meteor. Soc.*, **77**, 437-471.

Kiehl, J.T., J.J. Hack, and B.P. Briegleb, 1994: The simulated Earth radiation budget of the National Center for Atmospheric Research community climate model CCM2 and comparisons with the Earth Radiation Budget Experiment (ERBE). *J. Geophys. Res.*, 99, 20815-20827.

Lamb, P.J., 1978a: Large-scale tropical Atlantic surface circulation patterns associated with subsuharan weather anomalies. *Tellus,* **30**, 240-251.

Lamb, P.J., 1978b: Case studies of tropical Atlantic surface circulation pattern during recent sub-Sahara weather anomalies, 1967-1968. *Mon. Wea. Rev.*, **106**, 482-491.

Lamb, P.J., and R.A. Peppler, 1991: West Africa. *Teleconnections Linking Worldwide Climate Anomalies*. M. Glantz, R. Katz, and N. Nicholls, Eds, Cambridge University Press, 121-189.

Lacis, A.A., and J.E. Hansen, 1974: A parameterization for the absorption of solar radiation in the earth's atmosphere. *J. Atmos. Sci.*, **32**, 118-133.

Latif, M., and T.P. Barnett, 1995: Interactions of the tropical oceans. *J. Climate*, **8**, 952-964.

Latif, M., and A. Grötzner, 2000: The equatorial Atlantic oscillation and its response to ENSO. *Climate Dynamics*, **16**, 213-218.

Liu, T., X. Xie, W. Tang, H. Hu, 2002: Space based ocean surface wind vectors. Preceedings of the U.S. CLIVAR Atlantic Conference, 12-14 June 2001. Boulder Colorado, 6-8.

Lough, J. M., 1986: Tropical Atlantic sea surface temperatures and rainfall variations in Subsaharan Africa. *Mon. Wea. Rev.*, **114**, 561-570.

Mechoso, C.R., and coauthors, 1995: The seasonal cycle over the tropical Pacific in coupled ocean-atmosphere general circulation models. *Mon. Wea. Rev.*, **123**, 2825-2838.

Meehl, G.A., and J.M. Arblaster, 1998: The Asian-Australian monsoon and El Niño-Southern Oscillation in the NCAR climate system model. *J. Climate*, **11**, 1356-1385.

Mehta, V., 1998: Variability of the tropical ocean surface temperatures at decadal-multidecadal time scales, Part I: The Atlantic Ocean. *J. Climate*, **11**, 2351-2375.

Mellor, G.L., and T. Yamada, 1982: Development of a turbulence closure model for geophysical fluid problems. *Rev. Geophys. Space Phys.*, **20**, 851-875.

Mo, K.-C., and S. Häkkinen, 2001: Interannual variability in the tropical Atlantic and linkages to the Pacific. *J. Climate*, **14**, 2740-2762.

Moorhi, S., and M.J. Suarez, 1992: Relaxed Arakawa-Schubert: A parameterization of moist convection for general circulation models. *Mon. Wea. Rev.*, **120**, 978-1002.

Moura, A.D. and J. Shukla, 1981: On the dynamics of the droughts in northeast Brazil: Observations, theory and numerical experiments with a general circulation model. *J.Atmos. Sci.,* **38**, 2653-2675.

Neelin, J.D., and Coauthors, 1992: Tropical air-sea interaction in general circulation models. *Climate Dyn.*, **7**, 73-104.

Niiler, P.P., and E.B. Kraus, 1977: One-dimentional models of the upper ocean. *Modelling and Prediction of the Upper Layers of the Ocean*, E.B. Kraus, Ed., Pergamon, 143-172.

Nobre, P., and J. Shukla, 1996: Variations of sea surface temperature, wind stress, and rainfall over the tropical Atlantic and South America. *J. Climate*, **9**, 2464-2479.

Pacanowski, R.C., and S.G.H. Philander, 1981: Parameterization of vertical mixing in numerical models of tropical oceans. *J. Phys. Oceanogr.,* **11**, 1443-1451.

Palmer, T.N., G.J. Shutts, and R. Swinbank, 1986: Alleviation of a systematic westerly bias in general circulation and numerical weather prediction model through an orographic gravity wave parameterization. *Quart. J. Roy. Meteor. Soc.*, **112**, 1001-1039.

Robertson, A.W., and C.R. Mechoso, 2000: Interannual and interdecadal variability of the South Atlantic Convergence Zone. *Mon. Wea. Rev.*, **128**, 2947-2957.

Roeckner, E., J.M. Oberhuber, A. Bacher, M. Cristoph, I. Kirchner, 1995: ENSO variability and atmospheric response in a global coupled ocean-atmosphere GCM. *Max-Planck-Institut für Meteorology Report*, **178**.

Roy, C., and C. Reason, 2001: ENSO related modulation of coastal upwelling in the eastern Atlantic. *Progress in Oceanogr.*, **49**, 245-255.

Saravanan, R., and P. Chang, 2000: Interaction between tropical Atlantic variability and El Niño-Southern Oscillation. *J. Climate*, **13**, 2177-2194.

Schneider, E.K., B.P. Kirtman, Y, Fan, and Z. Zhu, 2001: Retrospective ENSO forecasts: The effect of ocean resolution. *COLA Tech. Report*, **109**, 27pp.

Schneider, E.K., Z. Zhu, B.S. Giese, B. Huang, B.P. Kirtman, J. Shukla, J.A. Carton, 1997: Annual cycle and ENSO in a coupled ocean-atmosphere model. *Mon. Wea. Rev.*, **125**, 680-702.

Schopf, P. S., and , A. Loughe, 1995: A reduced gravity isopycnal ocean model: Hindcasts of El Niño. *Mon. Wea. Rev.,* **123**, 2839-2863.

Schopf, P.S., and M.J. Suarez, 1988: Vacillations in a coupled ocean-atmosphere model. *J. Atmos. Sci.*, **45**, 549-566.

Shapiro, R., 1970: Smoothing, filtering and boundary effects. *Rev. Geophys. Space Phys.*, **8**, 359-387.

Servain, S., J. Picaut, and J. Merle, 1982: Evidence of remote forcing in the equatorial Atlantic Ocean. *J. Phys. Oceanogr.*, **12**, 457-463.

Smith, T.M., R.W. Reynolds, R.E. Livezey, and D.C. Stokes, 1996: Reconstruction of historical sea surface temperatures using empirical orthogonal functions. *J. Climate*, **9**, 1403-1420.

Tanimoto, Y., and S.-P. Xie, 1999: Ocean-atmosphere variability over the Pan-Atlantic basin. *J. Met., Soc., Japan,* **77**, 31-46.

Thompson, D.W.J., and J.M. Wallace, 2000: Annular modes in the extratropical circulation. Part I: Month-to-month variability. *J. Climate*, **13**, 1000-1016.

Thompson, D.W.J., J.M. Wallace, and G. Hegerl, 2000: Annular modes in the extratropical circulation. Part II: Trends. *J. Climate*, **13**, 1018-1036.

Tiedtke, M., 1984: The effect of penetrative cumulus convection on the large-scale flow in a general circulation model. *Beitr. Phys. Atmos.*, **57**, 216-239.

Tourre, Y., M.B. Rajagopalan, and Y. Kushnir, 1999: Dominant patterns of climate variability in the Atlantic Ocean region during the last 136 years. *J. Climate*, **12**, 2285-2299.

Venegas, S.A., L.A. Mysak, and D. Straub, 1997: Atmosphere-ocean coupled variability in the South Atlantic. *J. Climate*, **10**, 2904-2920.

Wagner, R.G., and A. da Silva, 1994: Surface conditions associated with anomalous rainfall in the Guinea coastal region. *Int. J. Climatol.*, **14**, 179-199.

Wallace, J.M., and D.S. Gutzler, 1981: Teleconnections in the geopotential height field during the Northern Hemisphere winter. *Mon. Wea. Rev.*, **109**, 784-812.

Ward, N., and C.K. Folland, 1991: Prediction of seasonal rainfall in the north Nordeste of Brazil using eigenvectors of sea surface temperature. *In. J. Clim.*, **11**, 711-743.

Williamson, D.L., J.T. Kiehl, and J.J. Hack, 1995: Climate sensitivity of the NCAR Community Climate Model (CCM2) to horizontal resolution. *Climate Dyn*, **11**, 377-398.

Wu, L., and Z. Liu, 2002: Is tropical Atlantic variability driven by the North Atlantic Oscillation? *Geophys. Res. Lett.*, **29**, 31-1-4.

Xie, S.-P., 1999: A dynamic ocean-atmosphere model of the tropical Atlantic decadal variability. *J. Climate*, **12**, 64-70.

Yu, Z., and P. S. Schopf, 1997: Vertical eddy mixing in the tropical upper ocean: its influence on zonal currents. *J. Phys. Oceanogr.*, **27**, 1447-1458.

Zebiak, S.E., 1993: Air-sea interaction in the equatorial Atlantic region. *J. Climate*, **8**, 1567-1586.

Zebiak, S.E., and M.A. Cane, 1987: A model El Niño-Southern Oscillation. *Mon. Wea. Rev.*, **115**, 2262-2278.

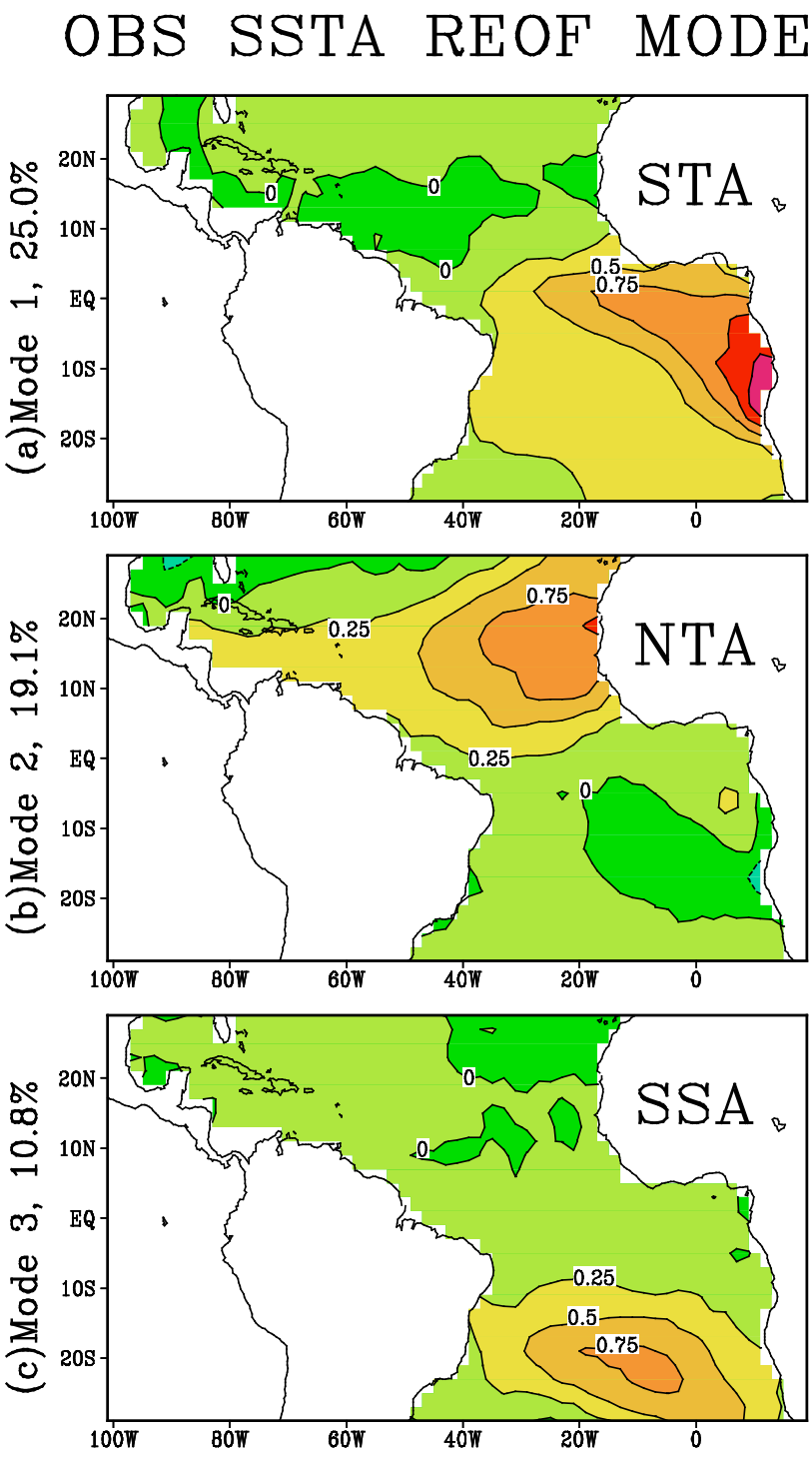

Figure 1. The spatial patterns of the (a) 1st, (b) 2nd, and (c) 3rd REOF modes of the seasonal mean SST anomalies for 1950-1998. The SST data are from U.S. Climate Prediction Center's analysis. The magnitude of the patterns corresponds to two times the standard deviation of the normalized time series. The contour interval is 0.25°C.

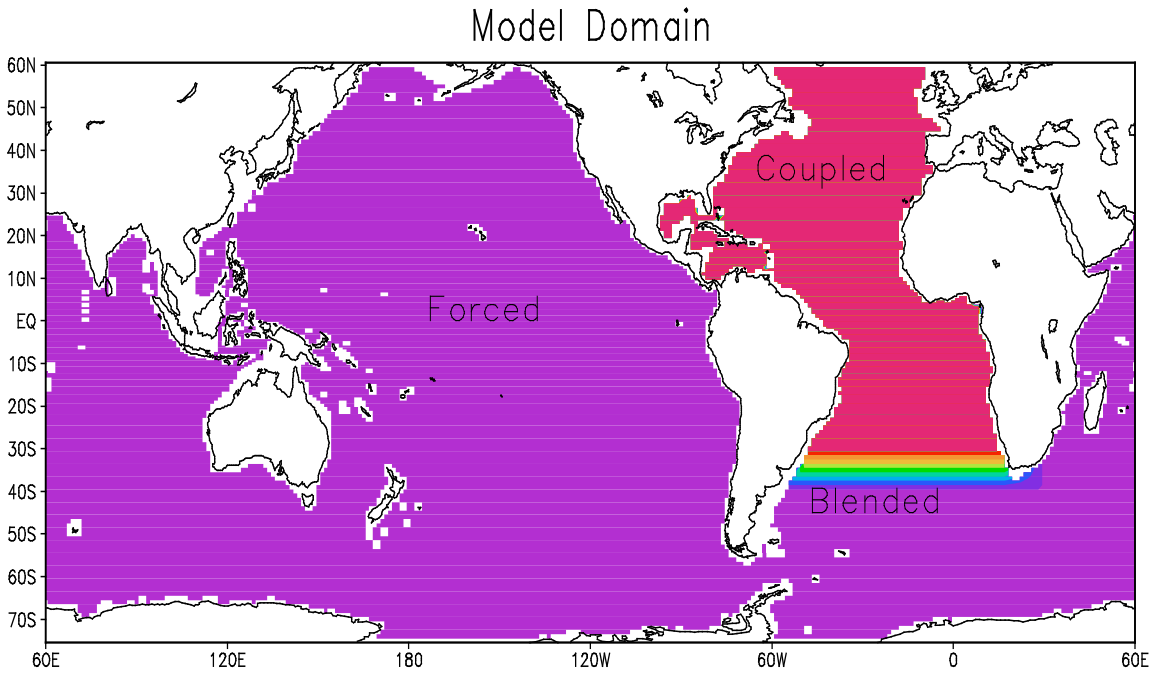

Figure 2. The regional coupling strategy over the oceanic domain. The fully coupled region is red. The rest of the oceanic region where the OGCM and the AGCM are forced with data is marked by purple color. The zonal belt over the South Atlantic with changing color is the blending zone.

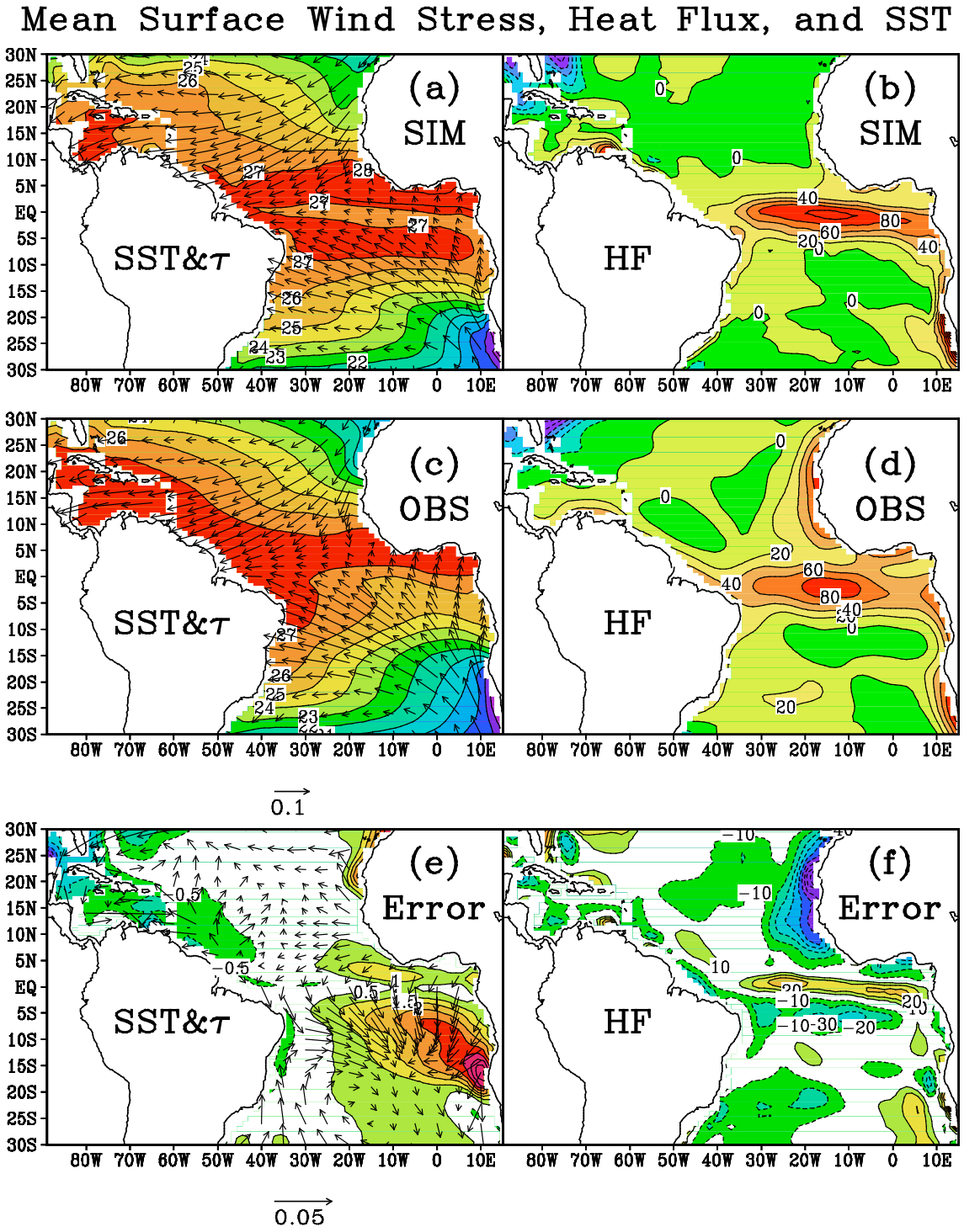

Figure 3. The annual mean state of (a) the SST and surface wind stress and (b) surface heat flux over the tropical Atlantic Ocean from the simulation. The same variables from the observations are shown in (c) and (d) respectively. The model error is shown (e) for the SST and surface wind stress and (f) surface heat flux. The contour intervals are 1°C for SST in (a) and (c), and 0.5°C for SST errors in (e). The contour intervals are 20Wm^{-2} for heat flux in (b) and (d), and10Wm^{-2} for heat flux error in (f). The arrow under panel (c) is 0.1 Nm^{-2}, representing the unit of vector in (a) and (c). The arrow under panel (e) is 0.05Nm^{-2}.

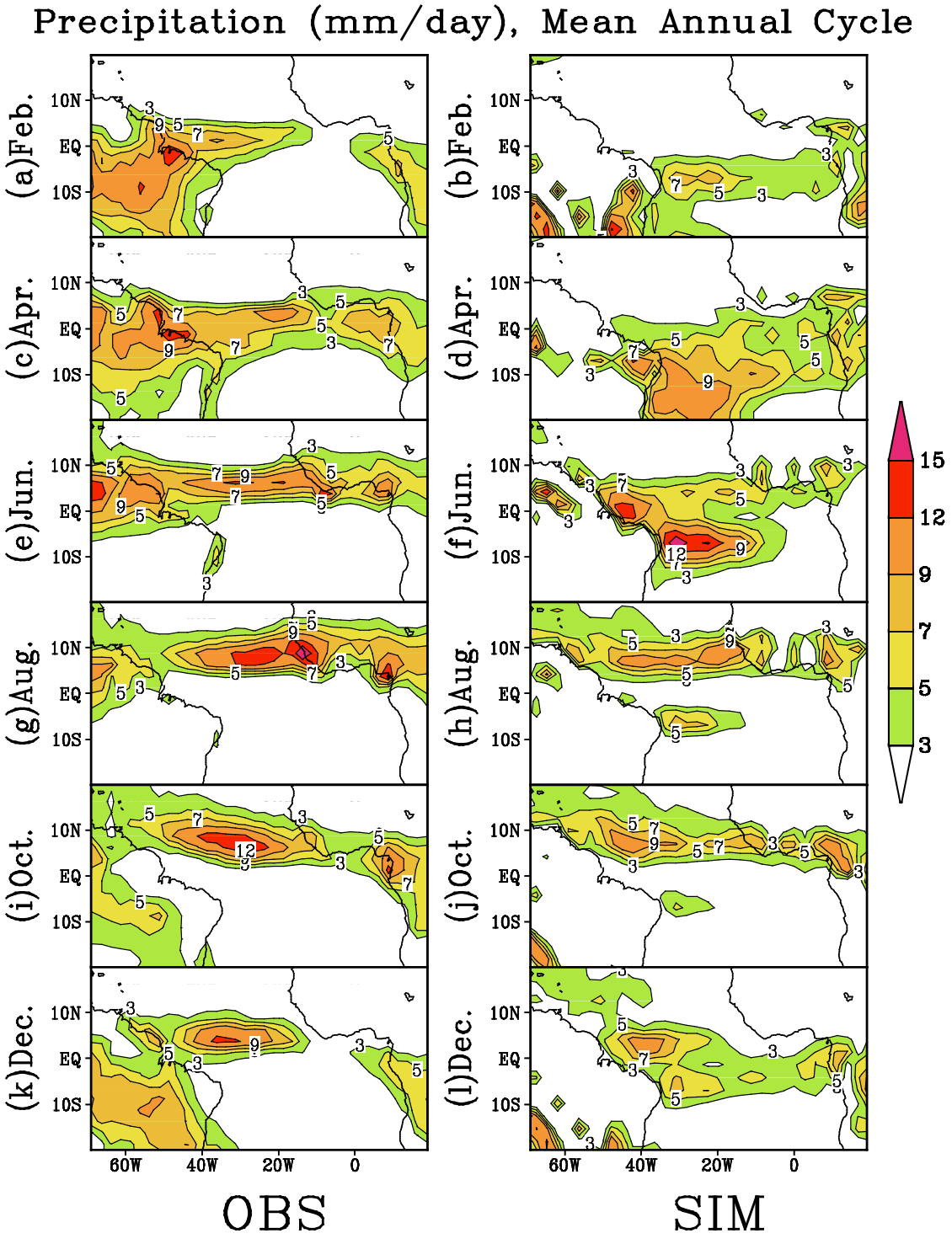

Figure 4. Climatological monthly precipitation over the tropical Atlantic region from the simulation and the CPC analysis. The fields are presented every other month from February to December. The observations are given in the left hand panels; the corresponding model results in the right hand panels. For each panel, the contour intervals are 3, 5, 7, 9, 12, and 15 mm day^{-1}.

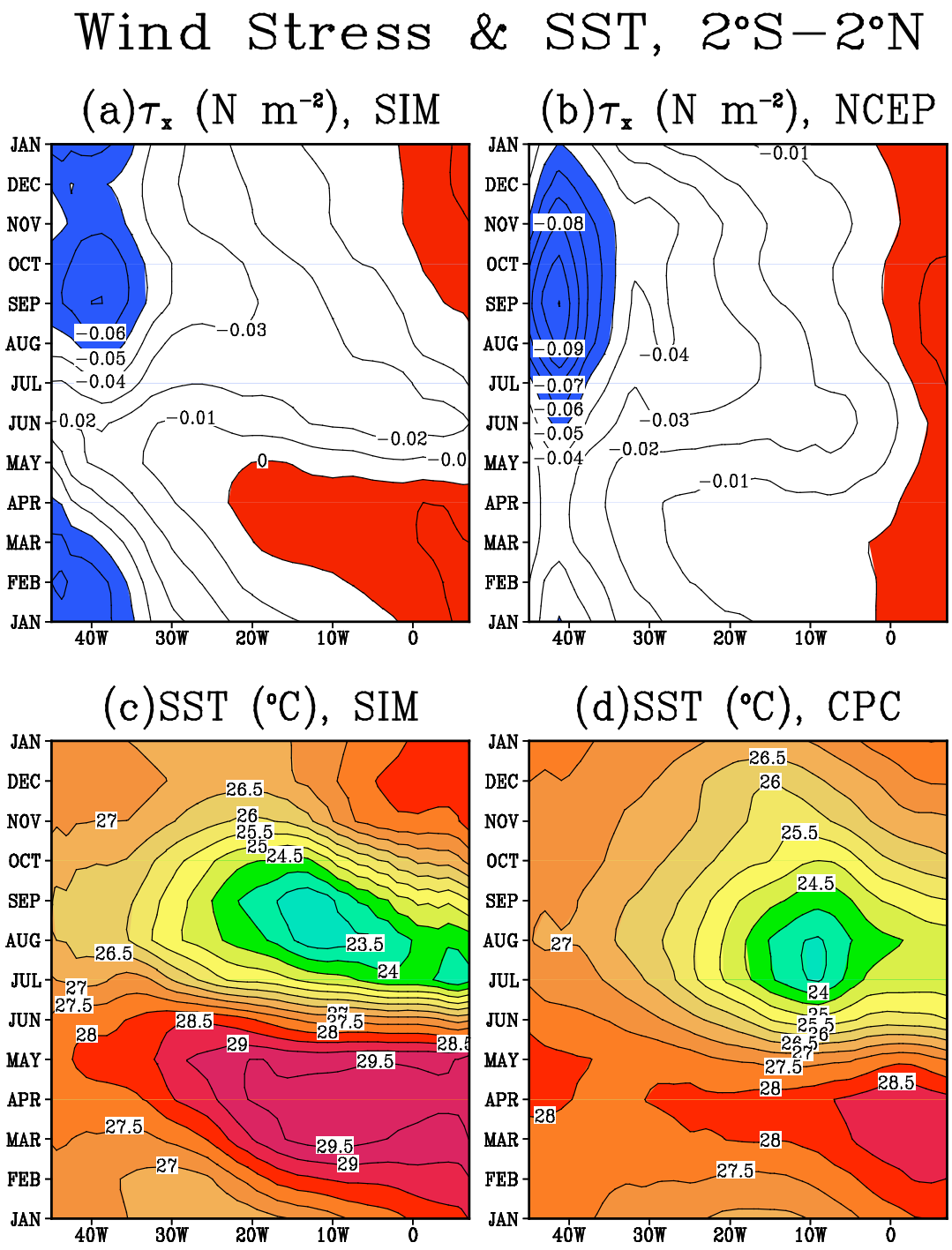

Figure 5. Time-longitude sections of the climatological monthly wind stress and SST averaged within 2°S-2°N over the Atlantic basin. The upper two panels are wind stress from (a) the simulation and (b) the NCEP reanalysis The lower two panels are SST from (c) the simulation and (d) the CPC analysis. The contour interval is 0.01 Nm^{-2} for the stress and 0.5°C for SST.

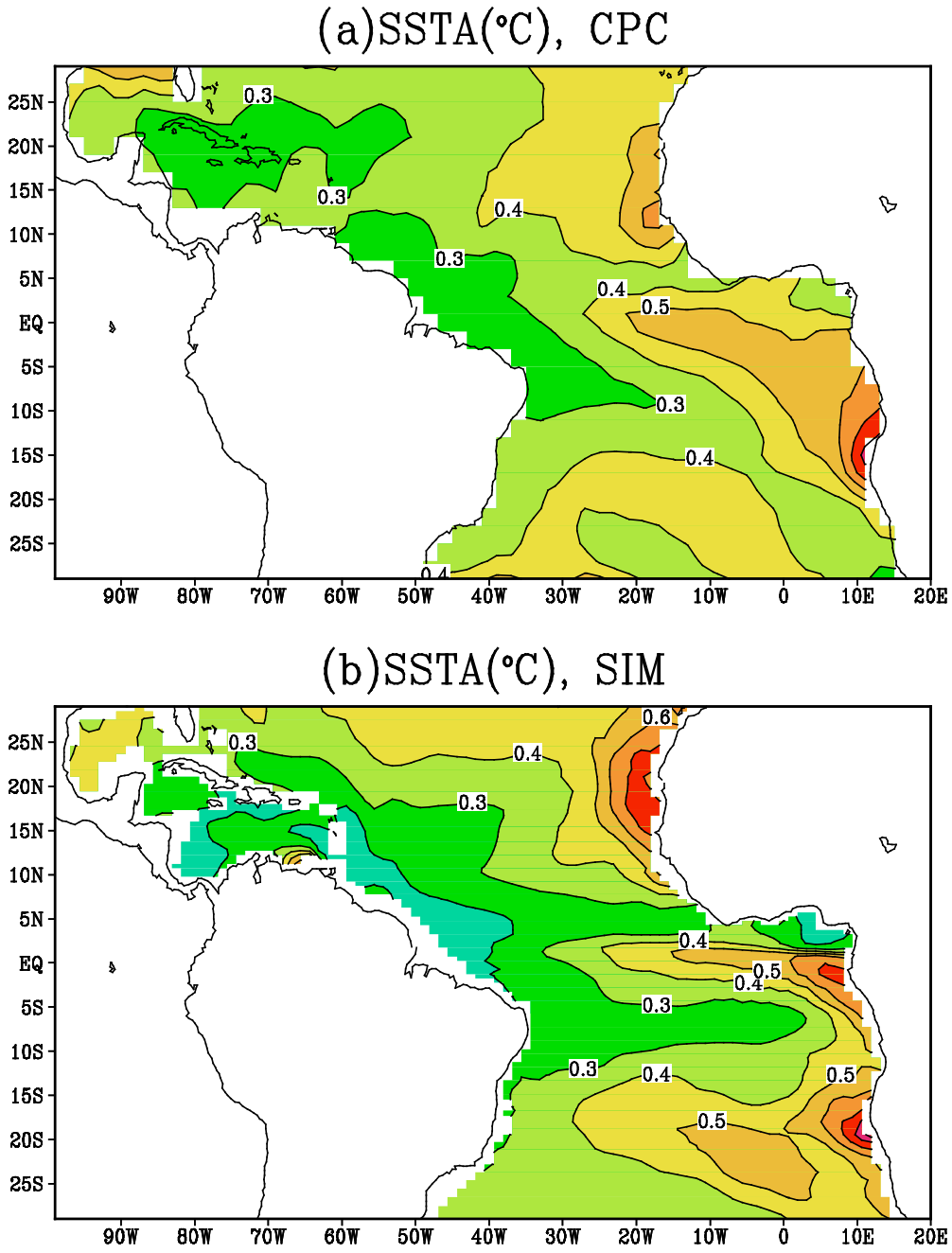

Figure 6. The spatial structure of the standard deviation of the seasonal mean SST anomalies from (a) CPC Analysis for 1950-1998 and (b) 110-year simulation of the regional CGCM. The contour interval is 0.1°C. The SST anomalies are seasonally averaged data.

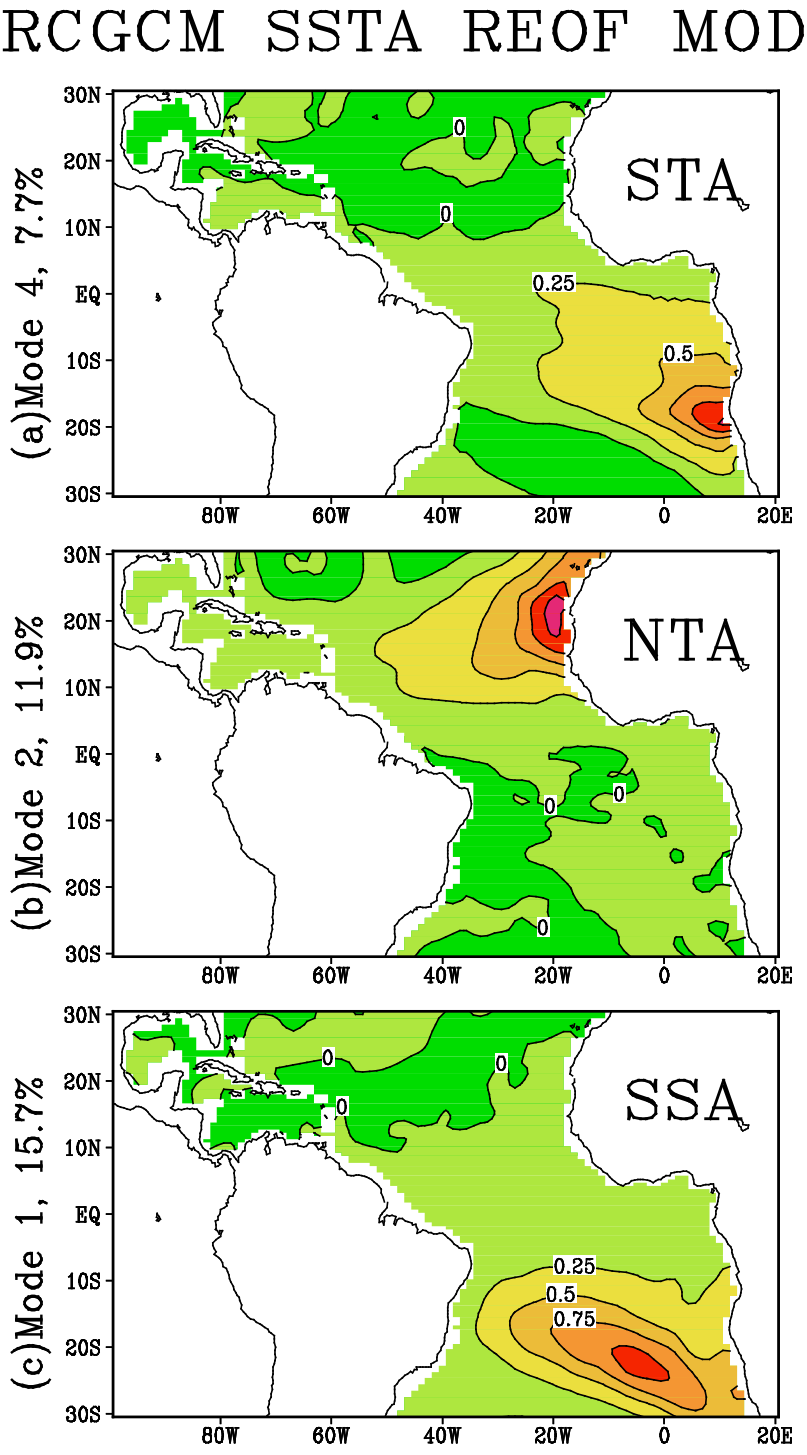

Figure 7. The spatial patterns of the (a) 4th, (b) 2nd, and (c) 1st REOF modes of the seasonal mean SST anomalies from the 110-year regional coupled GCM simulation. The magnitude of the patterns corresponds to two times the standard deviation of the normalized time series. The contour interval is 0.25°C.

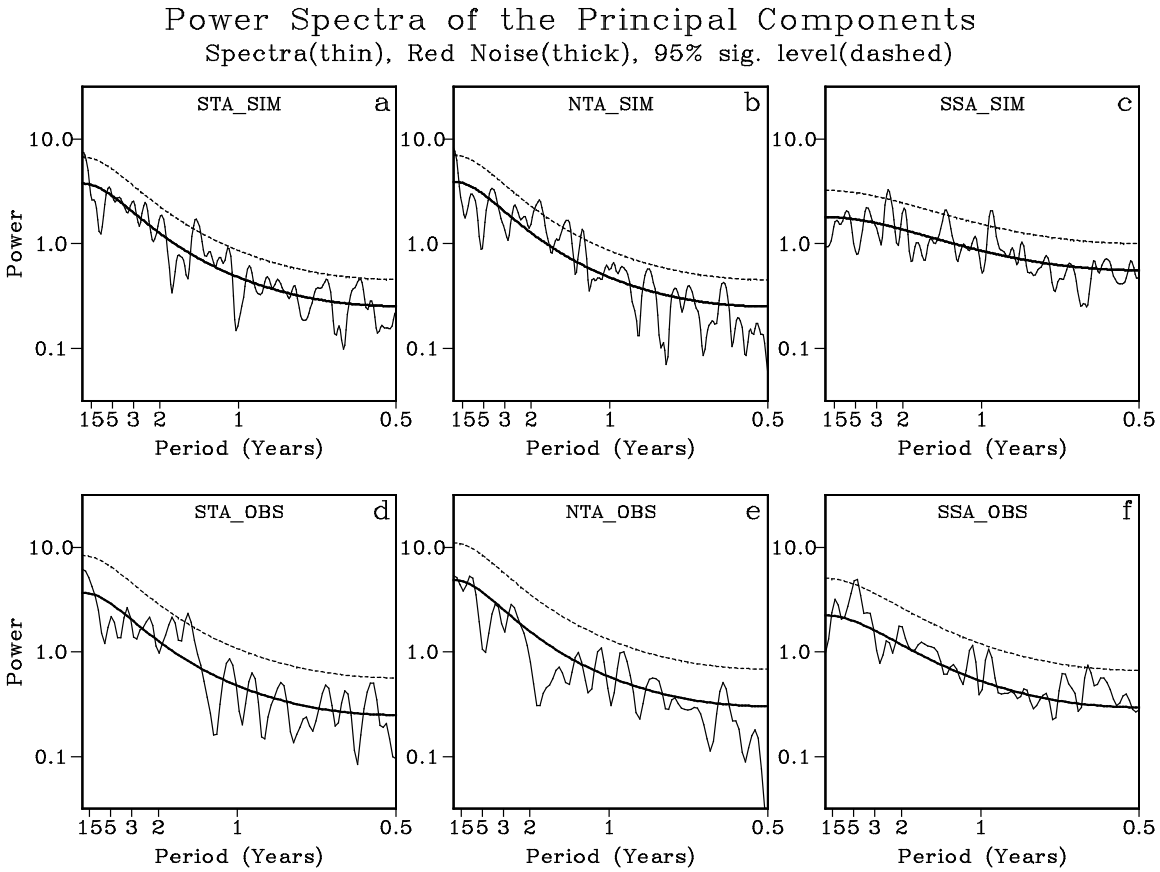

Figure 8. The upper panels are the power spectra of the time series of (a) the STA, (b) the NTA, and (c) the SSA modes from the seasonal data of the 110-year simulation. The lower panels (d,e,f) are the corresponding power spectra of these modes from 49-year (1950-1998) observational data.

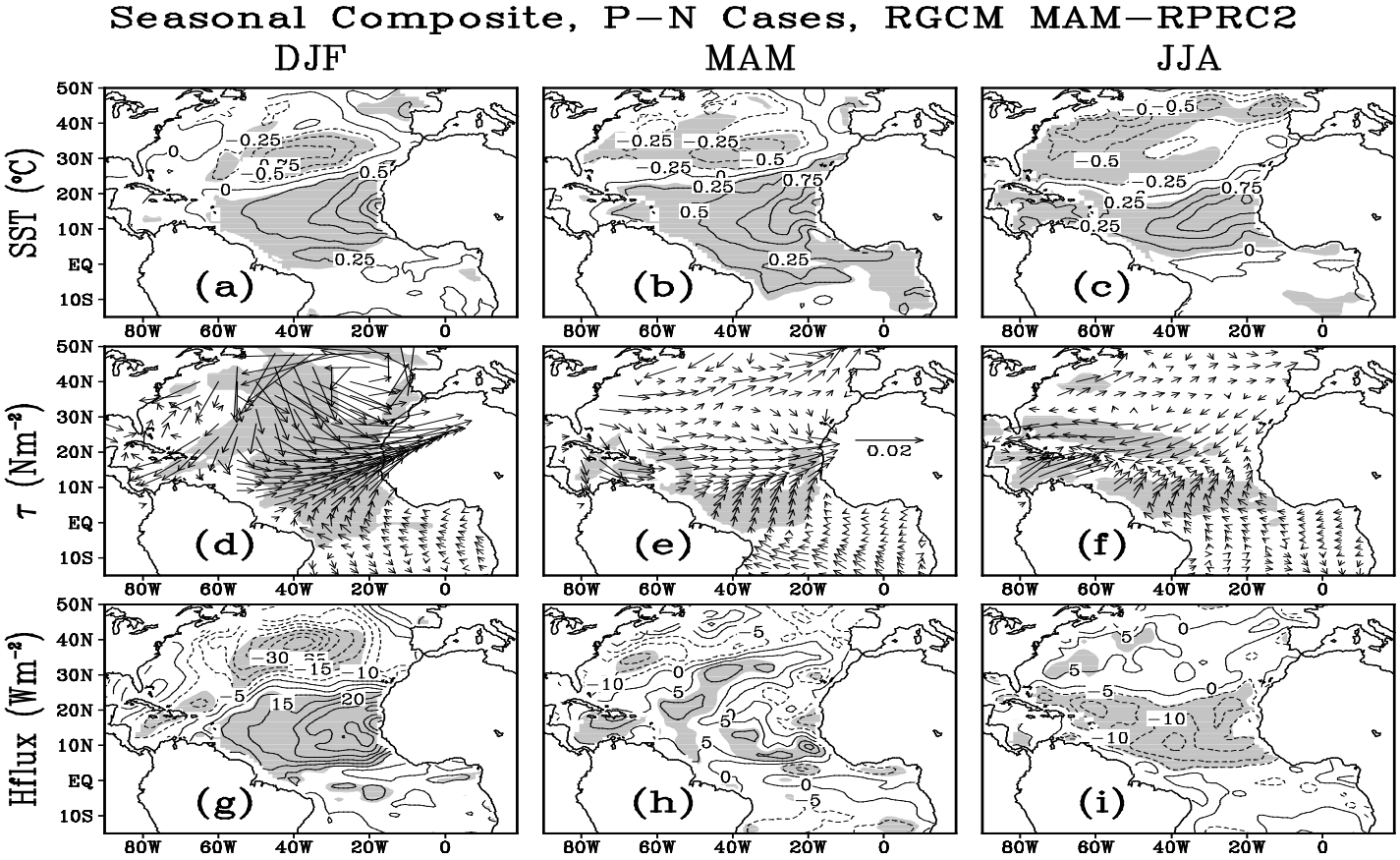

Figure 9. The differences of variables between the composite warm and cold NTA events from the simulation. The upper panels show the SSTA for (a) DJF, (b) MAM, and (c) JJA. The contour interval for these panels is 0.25°C. The middle panels show the surface wind stress anomalies for (d) DJF, (e) MAM, and (f) JJA. The unit arrow length on panel (e) is 0.02Nm^{-2}. The lower panels show the surface heat flux anomalies for (g) DJF, (h) MAM, and (i) JJA. The contour interval for these panels is 5Wm^{-2}. The shading shows the regions where the difference passes the 95% significance test.

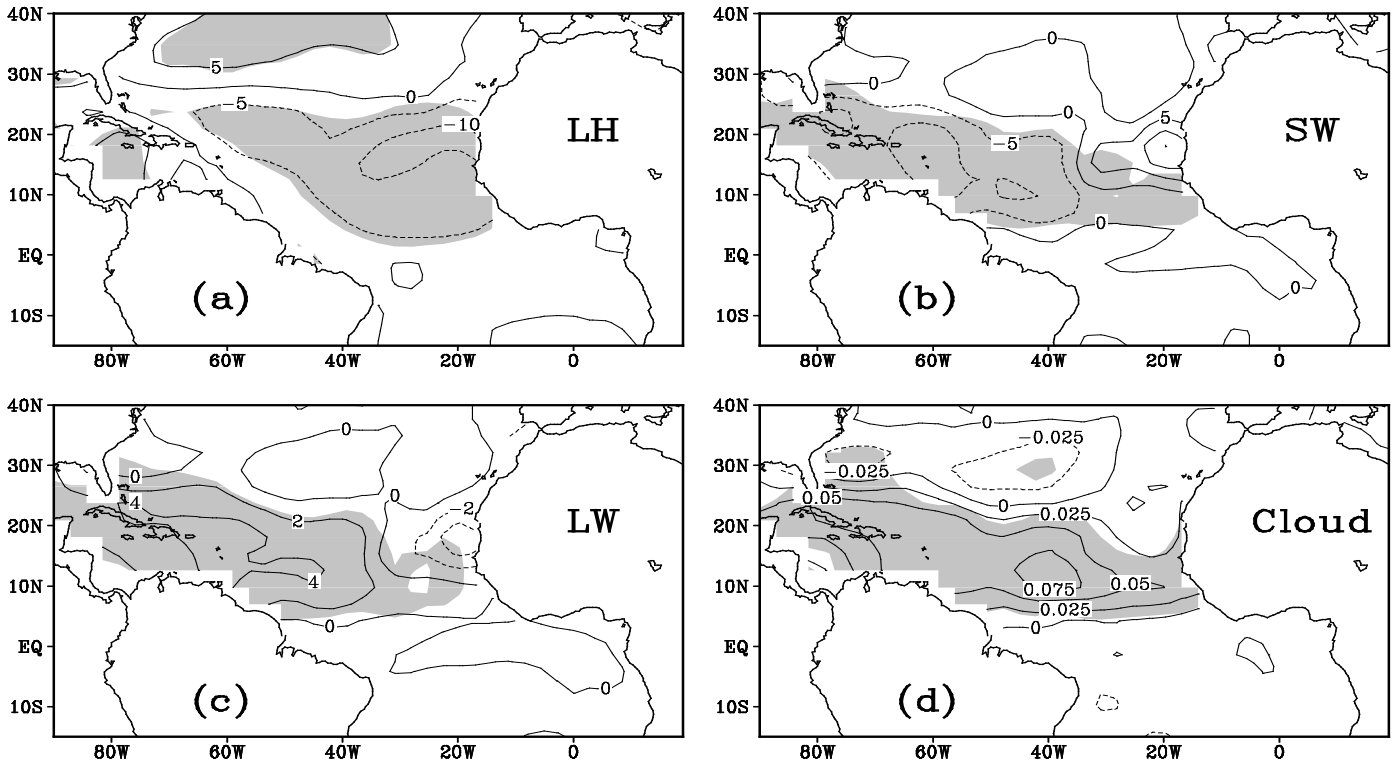

Figure 10. The difference of the heat flux components and cloud cover between the warm and cold NTA events in JJA from the simulation. Panel (a) and (b) are for the latent and short-wave radiative heat fluxes respectively. Their contour intervals are 5Wm^{-2}. Panel (c) is the long-wave radiative heat flux. Its contour interval is 2Wm^{-2}. Panel (d) is the cloud cover with contour interval of 0.025. The shading in all panels shows the regions that pass the 95% significance test.

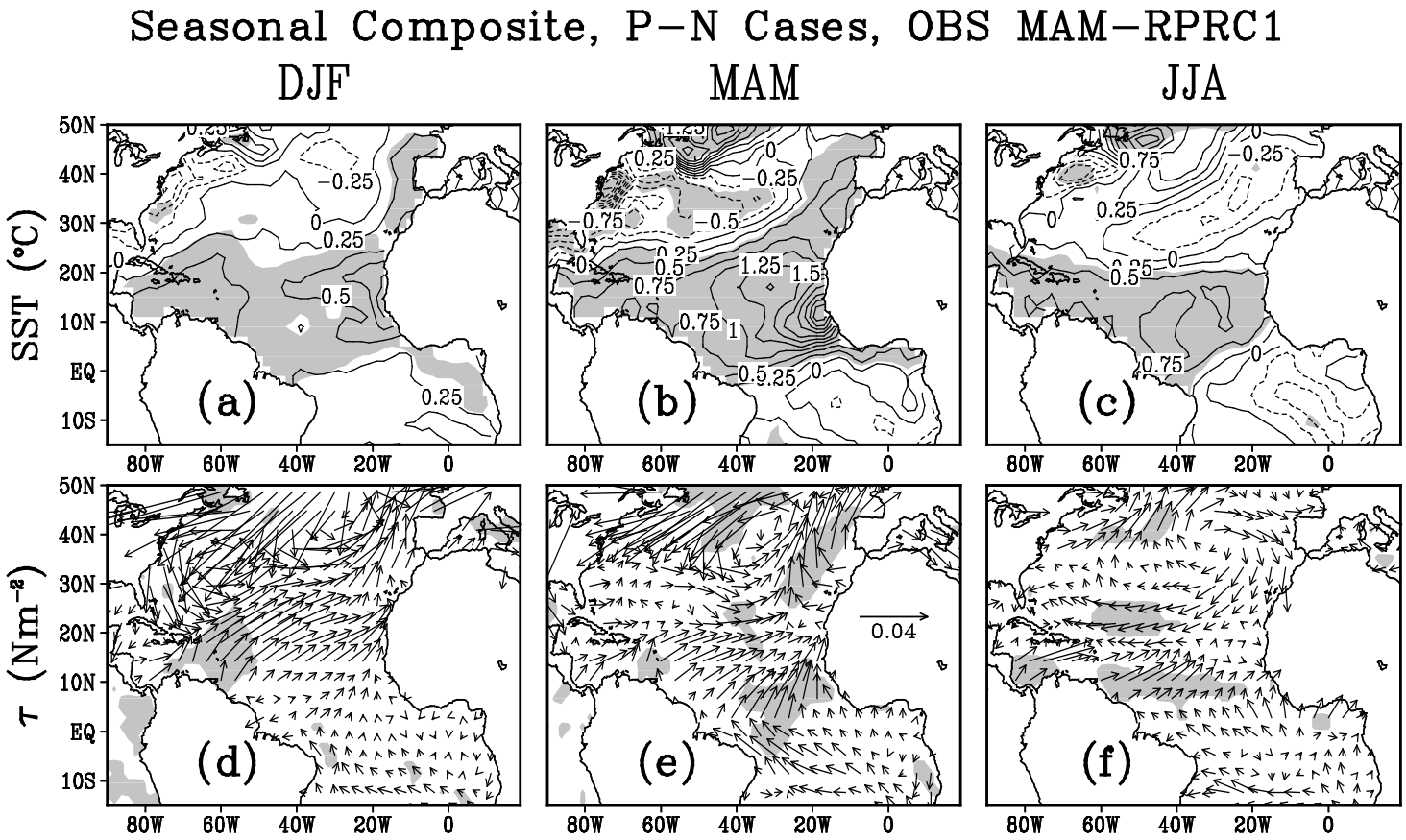

Figure 11. The differences of variables between the composite warm and cold NTA events from the simulation. The upper panels show the SSTA for (a) DJF, (b) MAM, and (c) JJA. The contour interval for these panels is 0.25°C. The lower panels show the surface wind stress anomalies for (d) DJF, (e) MAM, and (f) JJA. The unit arrow length on panel (e) is 0.04Nm^{-2}. The shading shows the regions where the difference passes the 95% significance test.

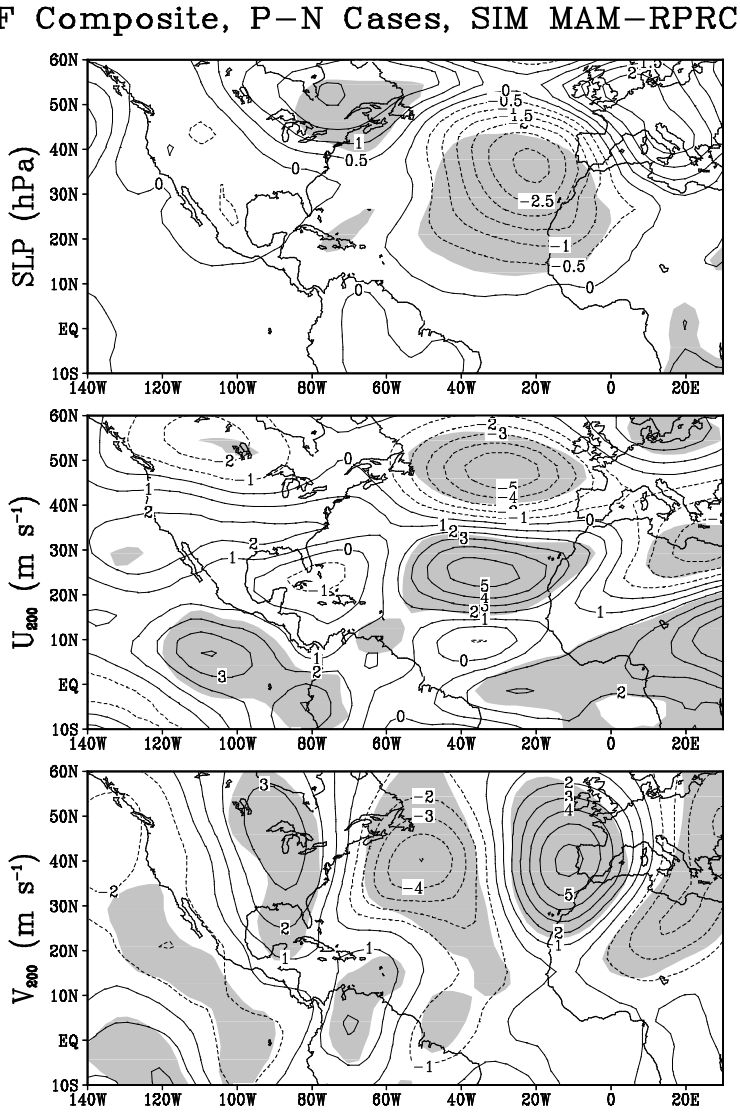

Figure 12. Differences of the atmospheric variables between the composite warm and cold NTA events. Panel (a) is SLP anomalies with contour interval of 0.5hPa. Panels (b) and (c) are zonal and meridional winds at 200hPa. Their contour intervals are both 1ms^{-1}. The shading on all panels shows the regions passing the 95% significance tests.

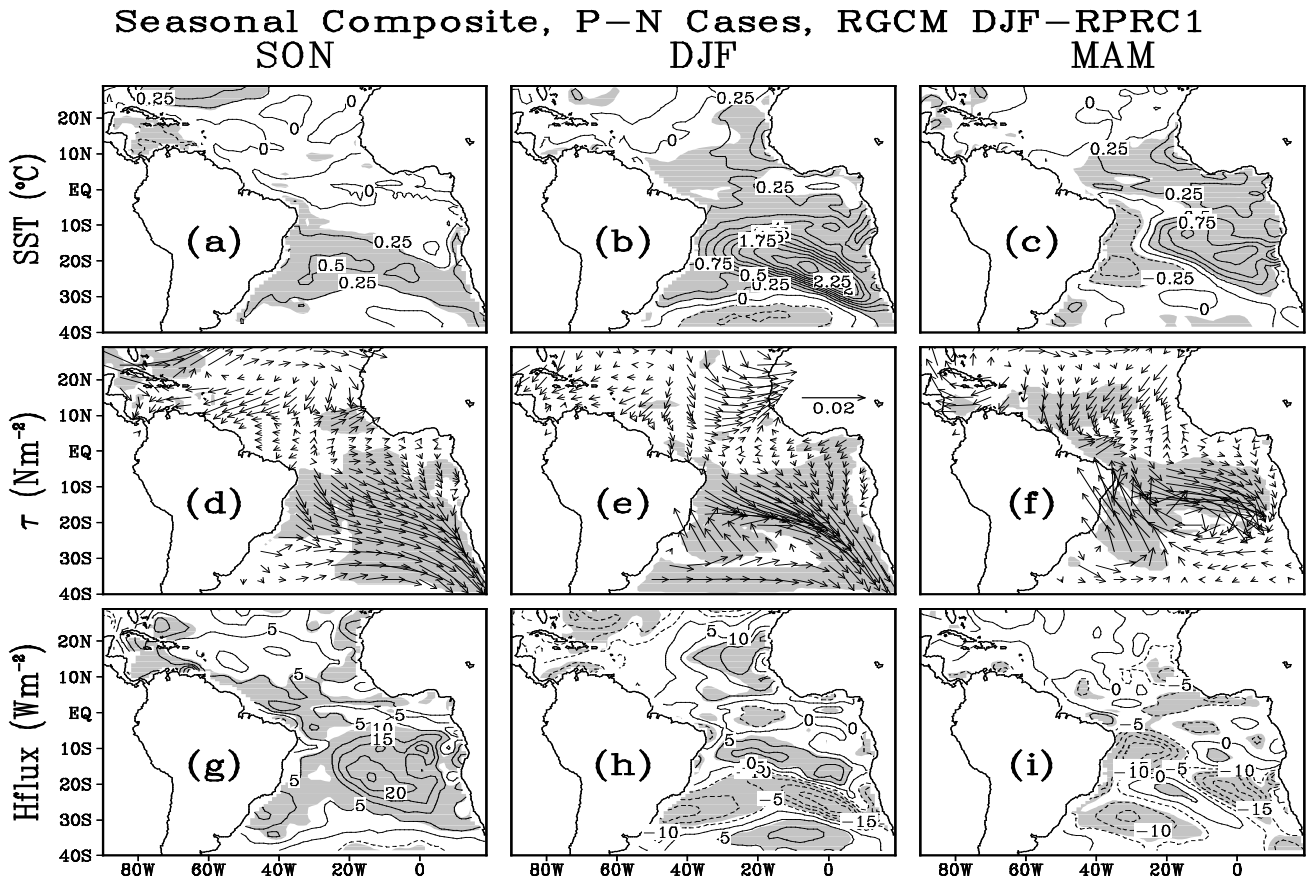

Figure 13. The differences of variables between the composite warm and cold SSA events from the simulation. The upper panels show the SSTA for (a) SON, (b) DJF, and (c) MAM. The contour interval for these panels is 0.25°C. The middle panels show the surface wind stress anomalies for (d) SON, (e) DJF, and (f) MAM. The unit arrow length on panel (e) is 0.02Nm^{-2}. The lower panels show the surface heat flux anomalies for (g) SON, (h) DJF, and (i) MAM. The contour interval for these panels is 5Wm^{-2}. The shading shows the regions where the differences pass the 95% significance test.

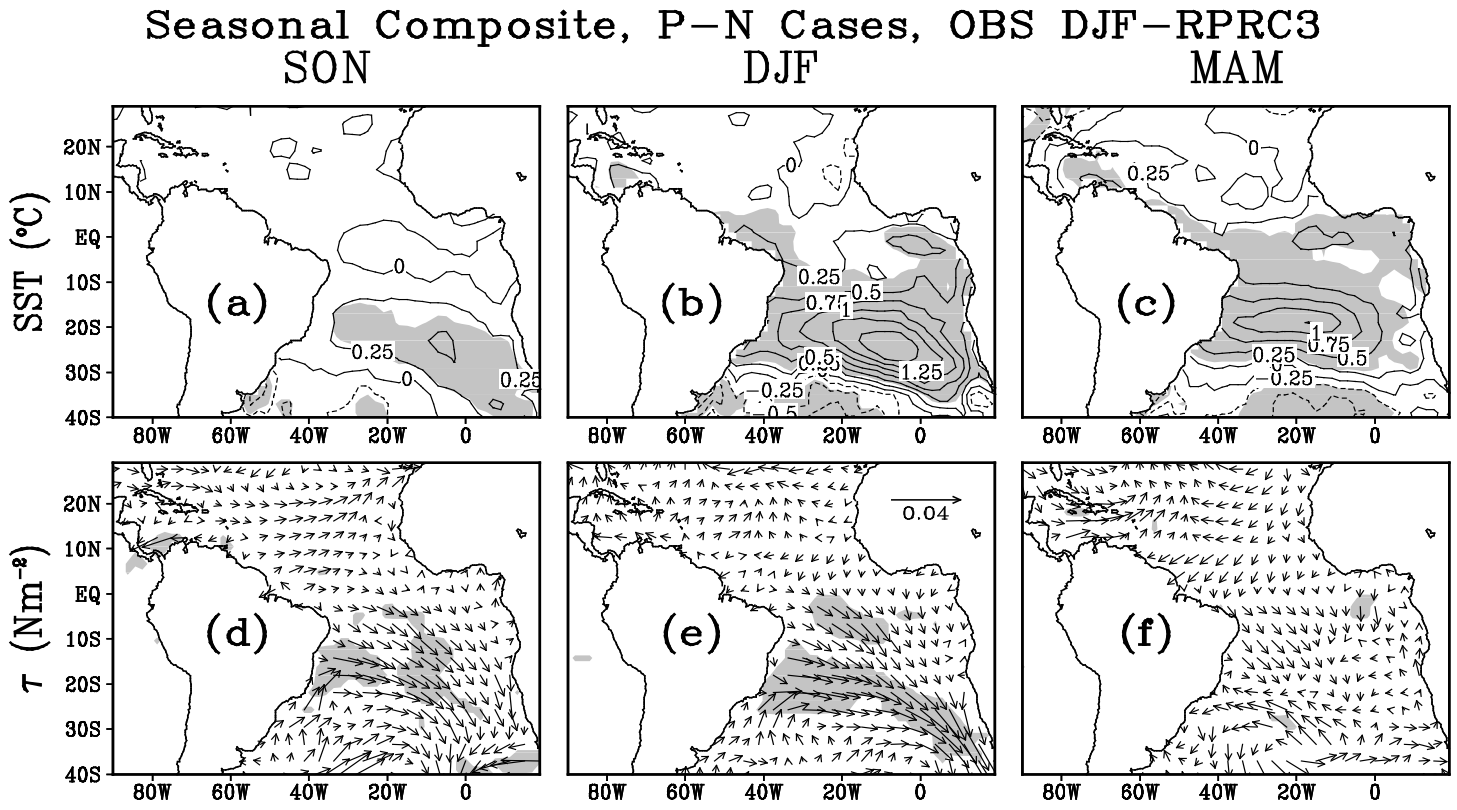

Figure 14. The differences of variables between the composite warm and cold SSA events from the observations. The upper panels show the SSTA for (a) SON, (b) DJF, and (c) MAM. The contour interval for these panels is 0.25°C. The lower panels show the surface wind stress anomalies for (d) SON, (e) DJF, and (f) MAM. The unit arrow length on panel (e) is 0.04Nm^{-2}. The shading shows the regions where the difference pass the 95% significance test.

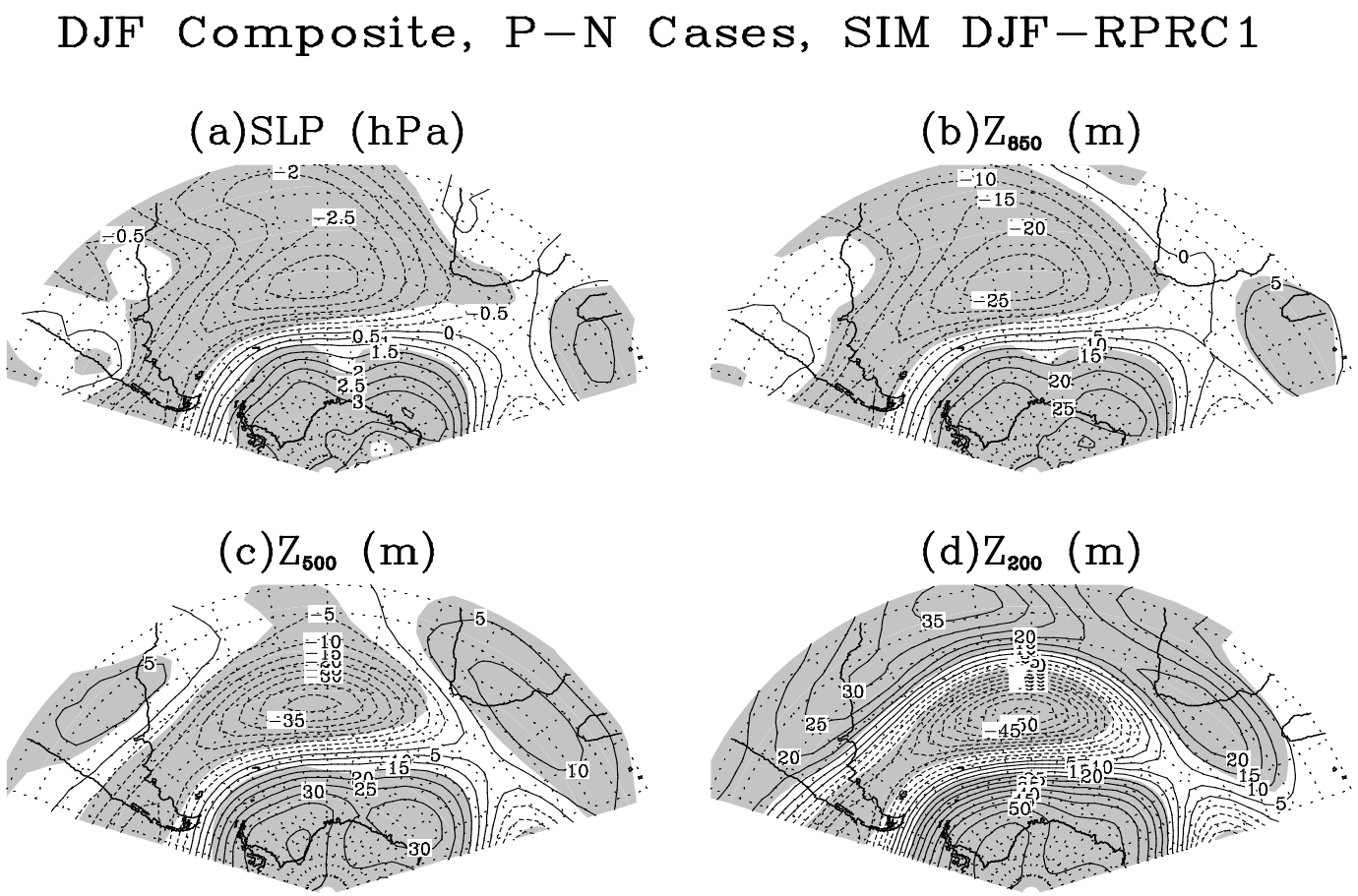

Figure 15. The DJF differences of (a) the SLP anomalies and the geopotential height anomalies at (b) 850hPa, (c) 500hPa and (d) 200hPa between the warm and cold SSA events from the simulation. The contour intervals are 0.5hPa for (a) and 5 meters for (b), (c), and (d). The shading shows the regions passing the 95% significance test.

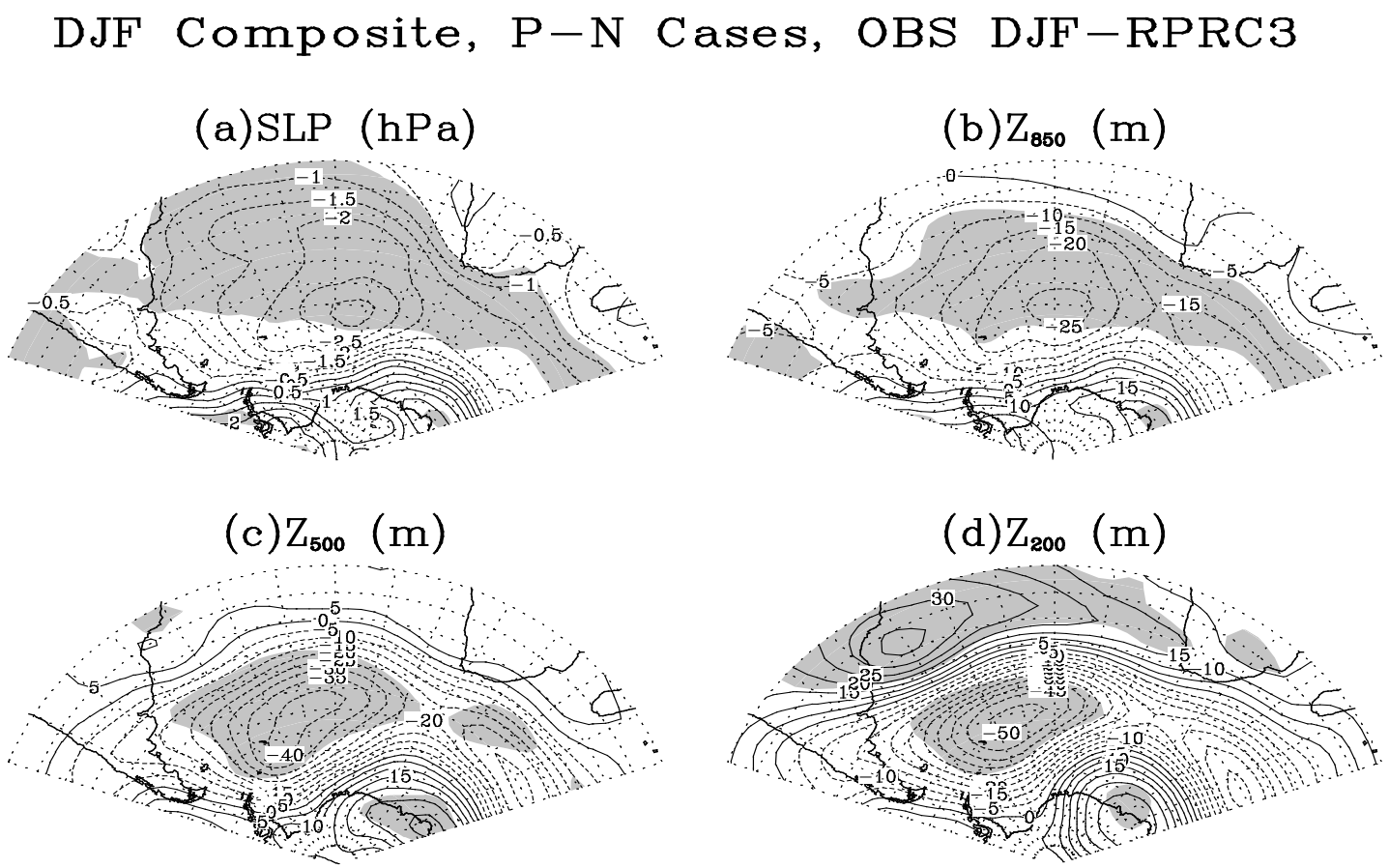

Figure 16. The DJF differences of (a) the SLP anomalies and the geopotential height anomalies at (b) 850hPa, (c) 500hPa and (d) 200hPa between the warm and cold SSA events from the observations. The contour intervals are 0.5hPa for (a) and 5 meters for (b), (c), and (d). The shading shows the regions passing the 95% significance test.

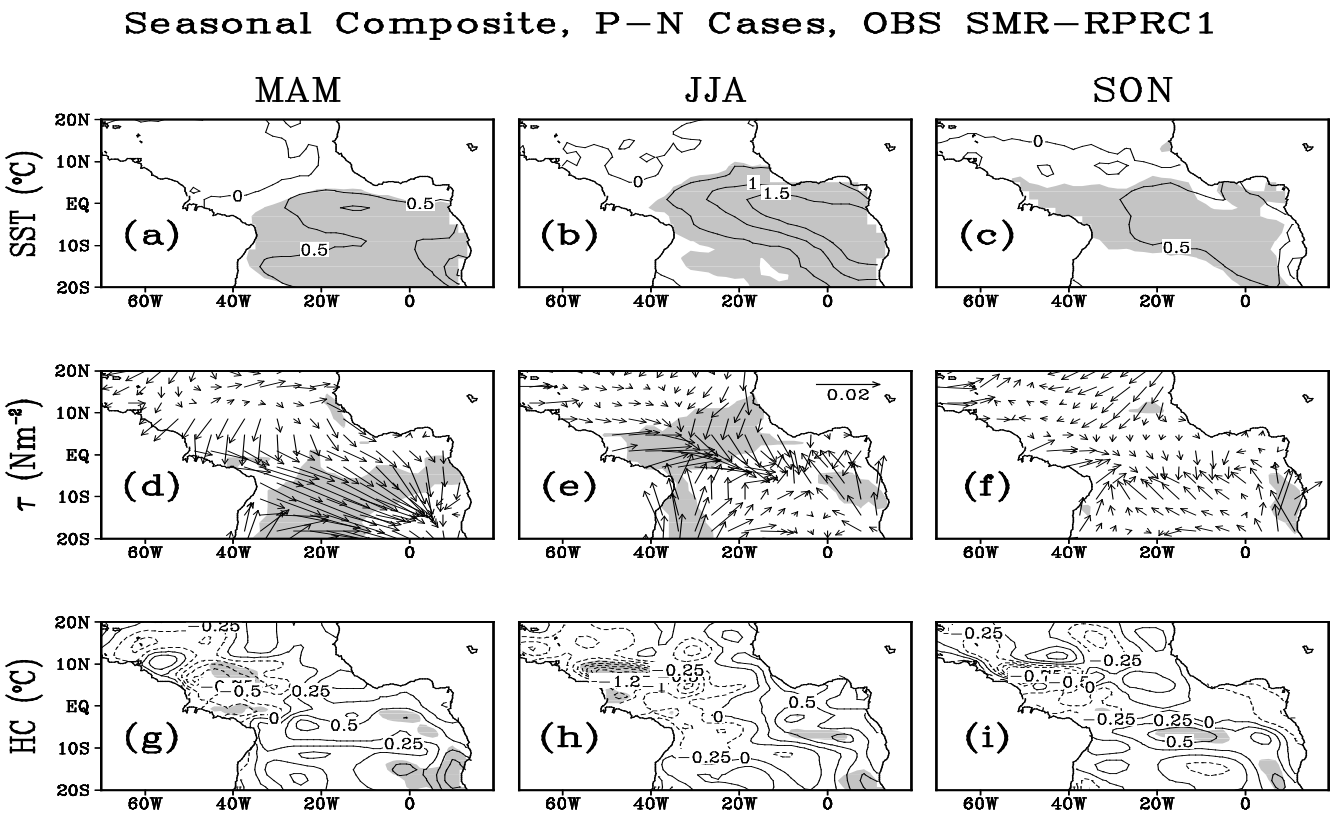

Figure 17. The differences of variables between the composite warm and cold STA events from the observations. The upper panels show the SSTA for (a) MAM, (b) JJA, and (c) SON. The contour interval for these panels is 0.5°C. The middle panels show the surface wind stress anomalies for (d) MAM, (e) JJA, and (f) SON. The unit arrow length on panel (e) is 0.02Nm^{-2}. The lower panels show the surface upper ocean heat content anomalies for (g) MAM, (h) JJA, and (i) SON. The contour interval for these panels is 0.25°C. The shading shows the regions where the differences pass the 95% significance test.

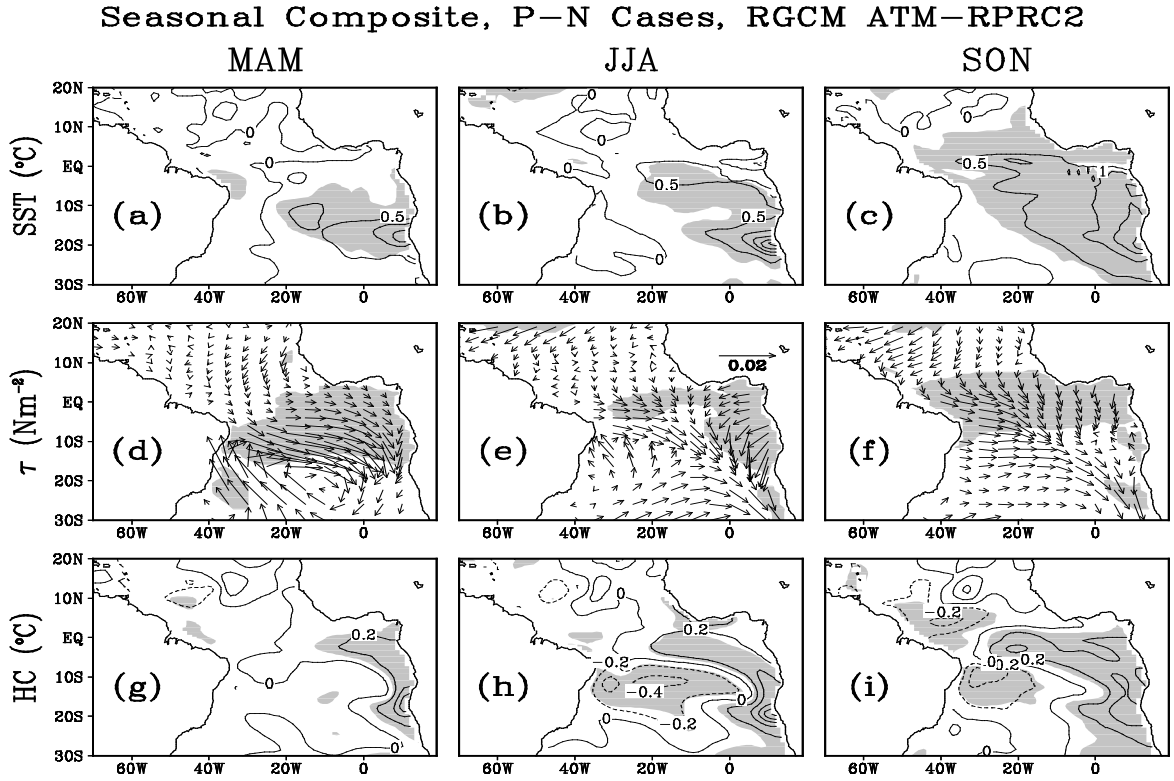

Figure 18. The differences of variables between the composite warm and cold STA events from the simulation. The upper panels show the SSTA for (a) MAM, (b) JJA, and (c) SON. The contour interval for these panels is 0.5°C. The middle panels show the surface wind stress anomalies for (d) MAM, (e) JJA, and (f) SON. The unit arrow length on panel (e) is 0.02Nm^{-2}. The lower panels show the surface upper ocean heat content anomalies for (g) MAM, (h) JJA, and (i) SON. The contour interval for these panels is 0.25°C. The shading shows the regions where the differences pass the 95% significance test.

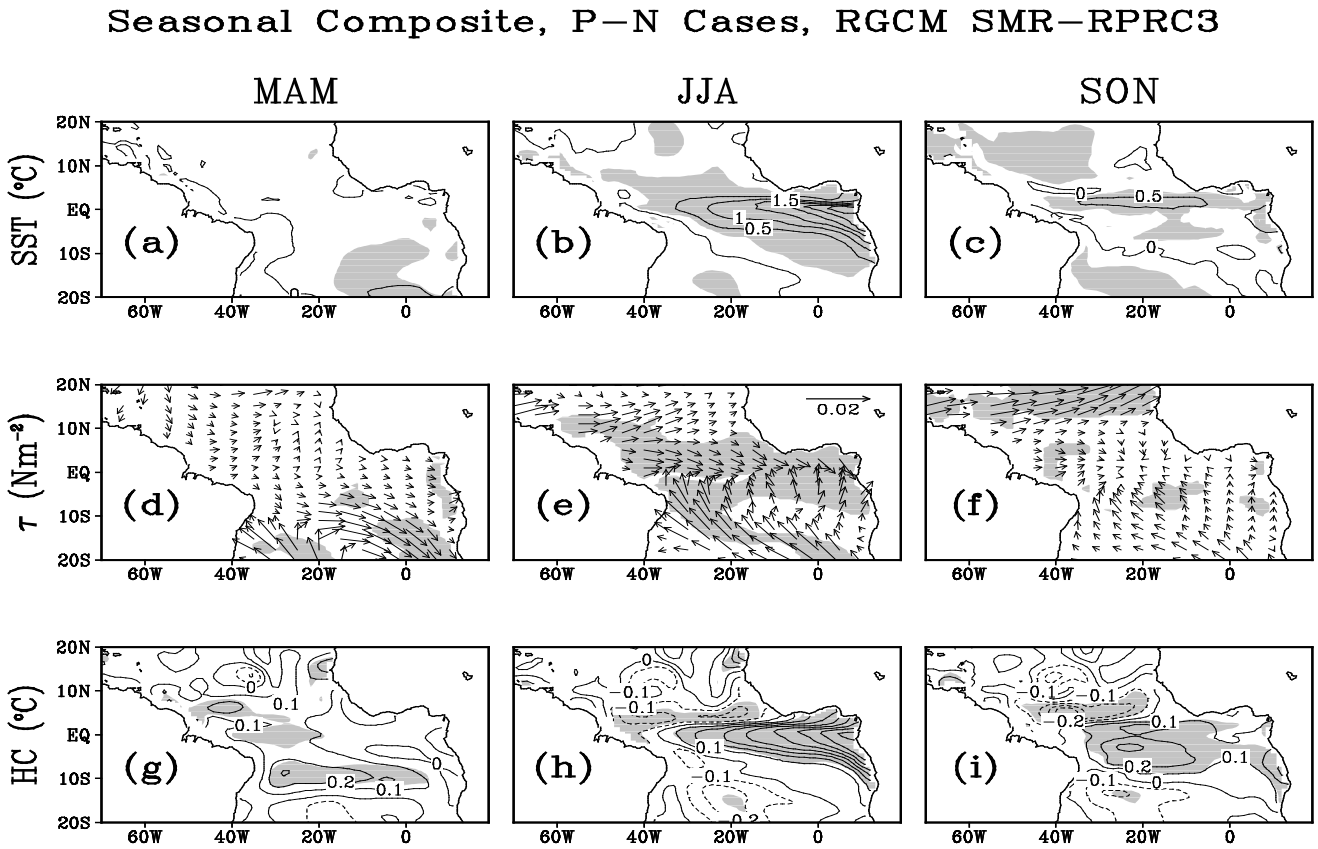

Figure 19. The differences of variables between the composite warm and cold events in the Gulf of Guinea from the simulation. The upper panels show the SSTA for (a) MAM, (b) JJA, and (c) SON. The contour interval for these panels is 0.5°C. The middle panels show the surface wind stress anomalies for (d) MAM, (e) JJA, and (f) SON. The unit arrow length on panel (e) is 0.02Nm^{-2}. The lower panels show the surface upper ocean heat content anomalies for (g) MAM, (h) JJA, and (i) SON. The contour interval for these panels is 0.25°C. The shading shows the regions where the differences pass the 95% significance test.